BAŞKENT UNIVERSITY
INSTITUTE OF SCIENCE AND ENGINEERING
DEPARTMENT OF DEFENSE TECHNOLOGIES AND SYSTEMS
MASTER'S OF DEFENCE PLATFORMS WİTH THESIS

THE EFFECT OF STACKING SEQUENCE OF CERAMIC ARMORS AND USE OF THIN PRELIMINARY LAYER ON BALLISTIC PERFORMANCE IN MULTILAYERED CERAMIC/COMPOSITE ARMOR SYSTEMS

BY

ŞÜKRÜ CÖMERT KİREMİTÇİ

MASTER OF SCIENCE THESIS

ANKARA – 2022

BAŞKENT UNIVERSITY
INSTITUTE OF SCIENCE AND ENGINEERING
DEPARTMENT OF DEFENSE TECHNOLOGIES AND SYSTEMS
MASTER'S OF DEFENCE PLATFORMS WİTH THESIS

THE EFFECT OF STACKING SEQUENCE OF CERAMIC ARMORS AND USE OF THIN PRELIMINARY LAYER ON BALLISTIC PERFORMANCE IN MULTILAYERED CERAMIC/COMPOSITE ARMOR SYSTEMS

BY

ŞÜKRÜ CÖMERT KİREMİTÇİ

MASTER OF SCIENCE THESIS

ADVISOR

PROF. DR. FARUK ELALDI

ANKARA – 2022

BAŞKENT UNIVERSITY

INSTUTE OF SCIENCE AND ENGINEERING

This study, which was prepared by Şükrü Cömert KİREMİTÇİ, for the program of Master's of Defense Platforms with Thesis, has been approved in partial fulfillment of the requirements for the degree of Master of Science in Defense Technologies and Systems Department by the following committee.

Date of Thesis Defense: 25/11/2022

Thesis Title: The Effect of Stacking Sequence of Ceramic Armors and Use of Thin Preliminary Layer on Ballistic Performance in Multilayered Ceramic/Composite Armor Systems

Examining Committee Member	**Signature**
Prof. Dr. Ömer Faruk Elaldı (Advisor) – Başkent Üniversitesi	……
Dr. Öğr. Üyesi Cenk Balçık – Başkent Üniversitesi	…….
Prof. Dr. Ahmet Hakan Argeşo – Atılım Üniversitesi	…….

APPROVAL

Prof. Dr. Faruk ELALDI

Director, Institute of Science and Engineering

Date: … / … / …….

BAŞKENT ÜNİVERSİTESİ

FEN BİLİMLERİ ENSTİTÜSÜ

YÜKSEK LİSANS / DOKTORA TEZ ÇALIŞMASI ORİJİNALLİK RAPORU

Tarih: 29 / 11 / 2022

Öğrencinin Adı, Soyadı : Şükrü Cömert KİREMİTÇİ

Öğrencinin Numarası : 21810177

Anabilim Dalı : Savunma Teknolojileri ve Sistemleri

Programı : Savunma Platformları Tezli Yüksek Lisans Programı

Danışmanın Unvanı/Adı, Soyadı : Prof. Dr. Faruk ELALDI

Tez Başlığı : The Effect of Stacking Sequence of Ceramic Armors and Use of Thin Preliminary Layer on Ballistic Performance in Multilayered Ceramic/Composite Armor Systems

Yukarıda başlığı belirtilen Yüksek Lisans tez çalışmamın; Giriş, Ana Bölümler ve Sonuç Bölümünden oluşan, toplam 86 sayfalık kısmına ilişkin, 29 / 11 / 2022 tarihinde tez danışmanım tarafından "Turnitin" adlı intihal tespit programından aşağıda belirtilen filtrelemeler uygulanarak alınmış olan orijinallik raporuna göre, tezimin benzerlik oranı % 15'tir. Uygulanan filtrelemeler:

1. Kaynakça hariç
2. Alıntılar hariç
3. Beş (5) kelimeden daha az örtüşme içeren metin kısımları hariç

"Başkent Üniversitesi Enstitüleri Tez Çalışması Orijinallik Raporu Alınması ve Kullanılması Usul ve Esaslarını" inceledim ve bu uygulama esaslarında belirtilen azami benzerlik oranlarına tez çalışmamın herhangi bir intihal içermediğini; aksinin tespit edileceği muhtemel durumda doğabilecek her türlü hukuki sorumluluğu kabul ettiğimi ve yukarıda vermiş olduğum bilgilerin doğru olduğunu beyan ederim.

Öğrenci İmzası: ……

ONAY

Tarih: … / … / 2022

Prof. Dr. Faruk ELALDI

ACKNOWLEDGEMENTS

First of all, I would like to thank my family, especially my brother Kerem KİREMİTÇİ, who always supported me during my thesis studies as in all areas of my life, my dear friend Canberk İNAN who encouraged me to continue my thesis studies in a busy work schedule, and my manager Serhat SUERİ who helped me from the beginning to the end of the process.

Moreover, I would like to thank Özgür ERDEM and Erdal DEMİR, who provided me with the opportunity to supply materials that I used in my studies, Kerem ÜSTÜN who helped me to prepare my test configurations and samples, Orhan Can YALÇIN, Esat BÖLÜKBAŞI, Cüneyt TUZLACIOĞLU and İbrahim Mert TUNÇ who allowed me to perform ballistic tests. Finally, I would like to thank my esteemed advisor Prof. Dr. Faruk ELALDI for all his support and technical background from the beginning of my thesis studies till the end.

ABSTRACT

Şükrü Cömert KİREMİTÇİ

THE EFFECT OF STACKING SEQUENCE OF CERAMIC ARMORS AND USE OF THIN PRELIMINARY LAYER ON BALLISTIC PERFORMANCE IN MULTILAYERED CERAMIC/COMPOSITE ARMOR SYSTEMS

Başkent University Institute of Science and Engineering

Department of Defense Technologies and Systems

2022

Regardless of whether tactical wheeled or tracked, the most important and vital system of armored land vehicles is the armor system. It is essential to use an optimum armor design that will not both lose the maneuverability of the relevant armored land vehicle and threaten personnel safety. One of the prerequisites for usability is to produce a cost-effective solution in armor systems, as in every other issue. Ceramic and/or composite armors have been used instead of solid and thick aluminum or steel armors in order to stop these ballistic threats, which have developed due to the greater development of projectile and firearm technologies compared to armor technology, especially in recent years. With this beginning, various multi-layer armor system configurations were created and validated according to STANAG 4569. However various researches have been carried out and continue to be carried out, especially in the 21st century, about arranging these configurations with optimum cost and areal density by changing various parameters.

In this study, the effect of the arrangement of the ceramic armor layers on the ballistic performance in a multi-layer armor system with STANAG 4569 Level-3 protection level was analyzed. In addition, it has been evaluated to what extent the preliminary front layer used in armor systems will affect the ballistic performance in order to protect the ceramic armor layers from external factors. At the same time, both experimental studies were compared with analytical models and the armor configuration with the optimum areal density was tried to be obtained with both tests and analysis models, provided that the same ballistic protection level was maintained.

KEYWORDS: Ceramic Armors, Ballistic Performance, Multilayered Ceramic-Metal Armor System, Composite Armors

ÖZET

Şükrü Cömert KİREMİTÇİ

ÇOK KATMANLI SERAMİK/KOMPOZİT ZIRH SİSTEMLERİNDE SERAMİK KATMAN DİZİLİŞ SIRALAMASININ VE ÖN KATMAN KULLANIMININ BALİSTİK PERFORMANSA ETKİSİ

Başkent Üniversitesi Fen Bilimleri Enstitüsü

Savunma Teknolojileri ve Sistemleri Anabilim Dalı

2022

Tekerlekli ya da paletli olmaları gözetmeksizin, kuşkusuz zırhlı kara araçlarının en önemli ve hayati sistemi zırh sistemidir. Hem ilgili zırhlı kara aracının manevra kabiliyetini kaybettirmeyecek hem de personel güvenliğini tehdit etmeyecek optimum zırh tasarımın kullanılması çok önemlidir. Her konuda olduğu gibi zırh sistemlerinde de maliyet etkin bir çözüm üretilmesi, kullanılabilirliğin ön koşullarından birisidir. Özellikle son yıllarda silah teknolojisinin zırh teknolojisine kıyasla daha fazla gelişmesi nedeniyle gelişen bu balistik tehditlerin durdurulabilmesi adına yekpare ve kalın alüminyum ya da çelik zırhlar yerine seramik ve/veya kompozit zırhlar kullanılmaya başlanmıştır. Bu başlangıç ile STANAG 4569'a göre çeşitli çok katmanlı zırh sistemi konfigürasyonları oluşturulmuş ve doğrulanmaya çalışılmıştır. Ancak, oluşturulan bu konfigürasyonların çeşitli parametreler değiştirilerek optimum maliyet ve alansal yoğunluğa sahip bir şekilde düzenlenmesi maksadıyla özellikle 21. yüzyılda çok çeşitli araştırmalar icra edilmiş ve edilmeye de devam edilmektedir.

Yapılan bu tez çalışmasında, STANAG 4569'a Seviye-3 koruma seviyesine sahip çok katmanlı bir zırh sisteminde seramik zırh katmanlarının diziliş sıralamasının balistik performansa etkisi analiz edilmiştir. Ayrıca, seramik zırh katmanlarının dış etmenlerden korunabilmesi için zırh sistemlerinde kullanılan ön katmanın balistik performansa etkinin ne ölçüde olacağı değerlendirilmiştir. Aynı zamanda, her iki deneysel çalışmaya konu olan konfigürasyonlar analitik modeller ile kıyaslanmış ve aynı balistik koruma seviyesini korumak şartıyla en optimum alansal yoğunluğa sahip zırh konfigürasyonu gerek testler, gerekse de analiz modelleri ile elde edilmeye çalışılmıştır.

ANAHTAR KELİMELER: Seramik Zırhlar, Balistik Performans, Çok Katmanlı Seramik-Metal Zırh Sistemi, Kompozit Zırh

TABLE OF CONTENTS

Page

LIST OF TABLES

Page

LIST OF FIGURES

Page

LIST OF SYMBOLS AND ABBREVIATIONS

SiC	silicon carbide
B_4C	boron carbide
Al_2O_3	alumina
wt	weight
BFS	Back face signature
EDS	Energy-dispersive spectroscopy
FE	Finite element
IR	Infrared
Ave	Average
CPU	Central processing unit
HV	Vickers
BBD	Box-Behnken Design
MRA	Multiple Regression Analysis
vol	Volume
NATO	North Atlantic Treaty Organization
HRC	Rockwell
L/D ratio	Ratio of the flighted length of the screw to its outside diameter
DOP	Depth of penetration
EPDM	Ethylene Propylene Diene Monomer
CNC	Computer numerical control
KE	Kinetic energy
V_b, V_l	ballistic limit of the metallic layer
W	total work done
M, m_p	projectile mass
W_p	work done in plastic deformation,
W_d	dynamic work done,
W_b	dynamic work done in bending of perfect plastic beam.
b, r	radius of projectile
Y	yield strength
h_0	thickness
ρ	density of armor plate
V_0, v_0	impact velocity
L	nose length of projectile
V_r	residual velocity
a	parameter from the regression procedure
V_s	striking velocity
P	experimental constant
m^I	mass of the area of armors which is deformed during penetration
ρ_t	density of target
h_t	thickness of target.
z	constant value
d, d_0	diameter of projectile
v_s	speed of the residual projectile when it impacts the backing plate
E_{kb}	kinetic energy of the residual projectile
m_r	mass of the residual projectile
E_k	initial kinetic energy of the projectile
E_p	kinetic energy loss of the projectile when it impacts the ceramic tile

E_c	energy dissipation of the ceramic facing
Y_p	dynamic yield strength of the projectile
l_e	erosion length of the projectile
ζ	empirical constant
HEL	Hugoniot elastic limit
h_{c0}	initial thickness of the ceramic
ρ_p	density of the projectile
E_{cs}	energy dissipated by shear in ceramic facing
E_{cc}	energy dissipated by crushing in ceramic facing
τ_s	shear strength of the ceramic
d_p	diameter of projectile after deformation/mushrooming
θ	semi-angle of ceramic cone
h_c	critical thickness of the ceramic plate between shear and compress
k_1	ratio of projectile deformed diameter to its initial diameter
δ	reduction of cross-section area
F_{cc}	maximum compressive force resistive to the projectile motion
β_p	empirical constant
ρ_c	density of the ceramic facing plate
u	penetration velocity of projectile
k_2	ratio of penetration velocity to initial velocity

1. INTRODUCTION

Projectile and firearm technologies are developing rapidly. Therefore, inventions of new projectiles and guns are increasing day by day. Considering new technologies, velocity of bullets now can reach up to very high level. Combining that with other improvements such as new bullet materials etc., this also increases the amount of energy that bullet can carry associated with kinetic energy. It means that impact energy of the bullet to the target could be really high. Because of that reason, considering the current rise of armed conflicts which include more powerful armaments, the term "ballistic protection" has become more meaningful.

Nowadays, ballistic protection is very important nearly for every field of the life. Researches about ballistic protection have been carried out in many areas from fighter aircrafts to combat vehicles, from personal equipment to buildings. All around the world, national defense departments continue working on ballistic protection to gain advantages against developing weaponry/projectile technologies and ensure the safety of personnel. Also, an important part of financial resources are being on this subject.

Traditionally, armor systems were used as a monolithic structure. And typically, this monolithic structure was consisted of medium strength steel blocks which have low hardness characteristics. But, these kind of armor systems were really heavy because of the thickness values for protection against firearm threads. Ballistic protection capacity becomes meaningful only when it was considered with the term "mobility". With the enhancements in science, high/ultra-high hardness and lightweight armor plates were started to be used instead of low hardness and heavyweight steel blocks. For example, wrought-steel homogeneous armor plates (meeting the requirements of specification MIL-DTL-12560), quenched and tempered high-hardness wrought steel armor plates (meeting the requirements of specification MIL-DTL-46100) and ultra-high hardness steel armor plates (meeting the requirements of specification MIL-DTL-32332) are one of the most used armor materials as of steel in defense industry recently.

Also, aluminum alloys are one of the best options amongst armor systems. Since, aluminum armors are lighter compared to armor steels, it enhances mobility of the structure. Besides, corrosion resistance of aluminum armors are better than armor steels. If these properties are combined with good weldability characteristics, commonly, hulls and frames of structures are made by aluminum armors. Maneuverability, fuel economy and system performance of the structures are increased by using aluminum armors as a hull of structure.

Generally, 5083 (meeting the requirements of specification MIL-A46027) and 7039 (meeting the requirements of specification MIL-A46063) series of aluminum armors are being used in military applications. However, these armors may be inadequate when the ballistic threat increases. Because of that reason, for instance in combat vehicles and armored personnel carriers, aluminum armors generally are used with armor steels as a multi-layered armor system depends on technical specifications and weight limits.

Recently, ceramic materials are also being used as a ballistic protection armor due to features such as low density (light-weight), high toughness, high compression strength, high hardness and high modulus of elasticity etc. Generally, these kinds of ceramic materials which are silicon carbide (SiC), boron carbide (B_4C) and alumina (Al_2O_3) are used in armor systems. Since ceramic materials have high hardness properties than aluminums and steels, they are used for erosion of the projectiles. Eroded projectile carries less kinetical energy then the first time when it was fired. Projectile mostly lost its sharp edges when it begins to penetrate ceramic materials. This means impact energy of the projectile to the target decreases. But, ceramic armors are very fragile because of their mechanical properties. Mostly, ceramic armors start to break into pieces with the first contact with projectiles. Due to that, multi-hit performance of ceramic armors are low. In relation with that, ceramic armors generally use as the first layer with the protective front layer in multi-layered armor systems. It is hard to produce high-hardness ceramic armors as a monolithic plate since, press machine that can apply really high pressure is required for desired ceramic thicknesses. Ceramic armors are generally produced in a square and/or hexagonal geometry. Generally adhesives and/or epoxy materials of composites are used for making them to stay together. Additionally, in order to obtain high ballistic performance with ceramic armors, they must be made of high purity ceramic powders and also, they must contain low porosity. Since special production techniques under cautious composition control are required, ceramic armors are relatively more expensive than steel and aluminum.

One of the other most critical part of the armor systems is composite materials. Distinctive properties of composite materials are being light, being ductile, having high strength, having high shock resistance, being resistant to the high temperatures and having high wear resistance. Generally, glass, carbon, ceramic and/or aramid fibers (also known as Kevlar) are used in composite armors with related epoxies or metal/ceramic matrixes. Sometimes, woven fabrics are used instead of simple fibers in order to increase strength of the materials. This also provide practicality in production of composite materials. Mostly, composite armors are used as a second layer in armors systems. Because, after first layer,

impact energy of the eroded projectile is absorbed by composite armors with deformation observed on composite materials with respect to mechanical properties such as ductility and shock resistance. Fractures of both projectile and first layer material are inhibited by composite armors in the second layer. Besides, composites are used as a main structure in body armors due to their light weight and high strength properties. Since the production methods of the composite materials are complex and difficult, they are naturally expensive but they have significant effects in armor systems in terms of ballistic performance.

In terms of tests performed to determine the armor levels, the resistance of the armor to the kinetic energy is measured. The kinetic energy varies according to the projectile type that is fired to the target during the test. For example, the armor levels specified in STANAG 4569 standard (Protection Levels for Occupants of Armored Vehicles) require using projectiles starting from a diameter of 5.56 mm up to 30 mm. Depending on projectile type, the armor levels are classified from 1 to 6. There is also another standard for determination of ballistic resistance, called NIJ 0101.06 (Ballistic Resistance of Body Armor), for determination of the armor protection levels via information such as a different projectile velocity, firing angle and number of shots are defined in standard for each protection levels. This information is explained in the relevant standards. According to the results that are obtained from ballistic tests, protection levels of armor systems can be determined with respect to the criteria that was given in standard. There are also some tests for finding the maximum velocity of the non-perforated case and minimum velocity of the perforated case of the related projectile, which also called V50 test. Ballistic tests are generally performed with a gas or powder gun (barrel system) for shooting and a properly positioned plate holder at target location. The amount of powder to be placed in the barrel's chamber and/or the distance of the target should be adjusted for the required projectile velocity values specified in the standards. This has to be done by the pre-test shots before starting the ballistic test. Otherwise, the test results will not be valid.

Penetration process at ceramic based armors can be classified into three stages in multi-layered armor systems. First stage is breaking of ceramic layer, second stage is progressing of projectile in damaged ceramic tile and the last stage is deformation of backing plate. When projectile contacts with ceramic layer, stress waves are started to propagate from the impact surface and ceramic material starts to break and a conoid structure is observed which is also called ceramic conoid. It was given in Figure 1.1.

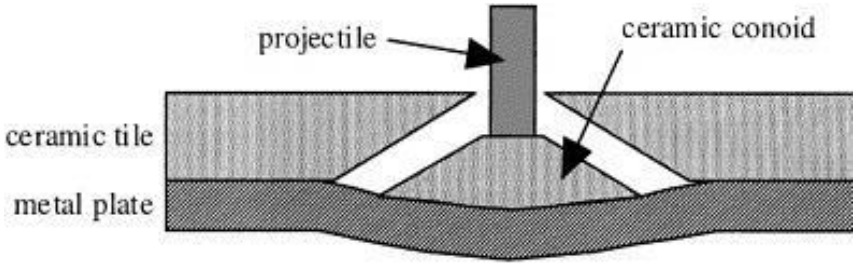

Figure 1.1. Ceramic Conoid [1]

Cone cracks and radial cracks start to occur during penetration. These cracks can be seen in Figure 1.2.

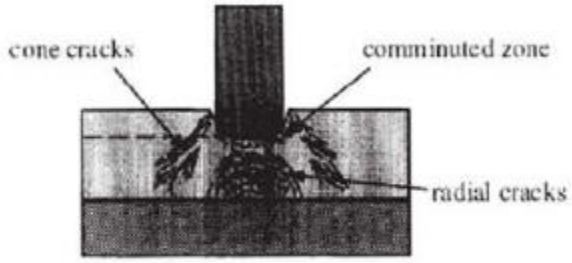

Figure 1.2. Cone and Radial Cracks in Ceramic Tile [1]

With the first contact of projectile with ceramic layer, projectile starts to lose its nose geometry and sharp edges, which are also called erosion. Kinetic energy of the projectile starts to reduce during the progressing in ceramic tile. At this moment, ceramic conoid which includes cracks, is accelerated along the impact direction. Pressure is distributed on the backing plate due to the accelerated ceramic conoid. As a result of that, deformation is occurred in the backing plate and projectile is stopped by target. Interlayers after ceramic layer (first layer) such as air, liquid etc. can be used for reducing the kinetic energy of the projectile in armor systems.

Regarding the developments in defense technologies and applications, researches are being carried out for increasing ballistic protection levels without compromising the performance and mobility. New ballistic armor systems are being developed against the growing powerful projectile technologies. Within this scope, studies are ongoing for producing lightweight and high-strength materials and ballistic tests are performed for validation of those materials.

2. LITERATURE SURVEY

Based on recent studies, it has been demonstrated that geometry of the target has significant effect on ballistic performance. By using different target geometries, stress distribution that caused by projectiles can be enlarged. Enlarging stress distribution raises the energy absorption rate of the related ballistic layer. For the application of the ceramics to armor vests, ceramic armor plates which have different geometries have been tested and validated according to the NIJ 0101.06 standard. Fundamentally, it was tried to enlarge the stress distribution area and by this, it was aimed to increase resistance of the ceramic armor to the dynamic load [2].

Alumina which contains 4 wt.% of niobia (Nb2O5) with two different geometries which are flat-faced and convex-faced, aluminum backing plate (5052 H34), aramid fabric which consists in a plain weave fabric composed by Kevlar 29 fibers with areal density of 450 g/m2 and clay witness which simulating the consistency of the human body (validated by the drop weight test) were used in tests by Braga, Luz Monteiro and Lima [2]. Ballistic test was evaluated according to the back-face signature (BFS) methodology that was specified in NIJ 0101.06 standard. 7.62 x 51 mm M1 projectiles were used and impact velocity of each projectile was measured by using a HPI B472 optical barrier. Shapes and characteristics of materials used in tests were given below in Figure 2.1, Table 2.1 and Table 2.2 [2].

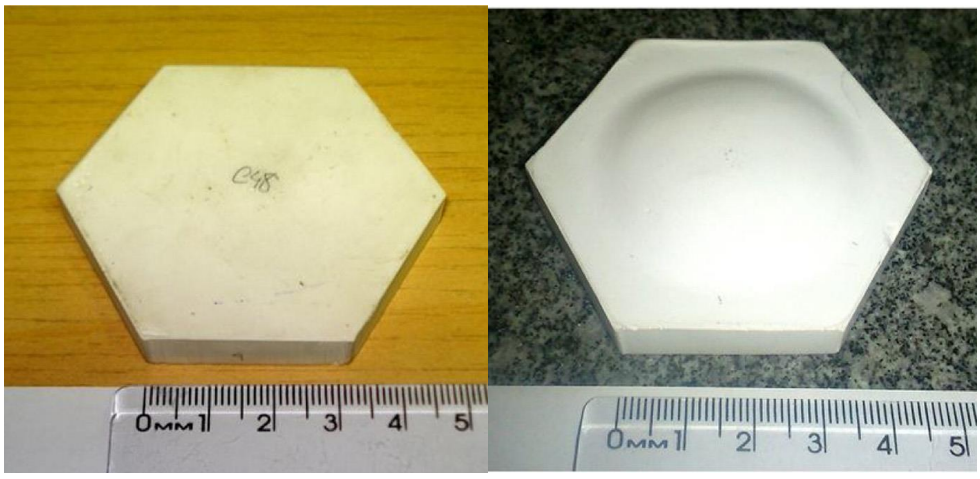

Figure 2.1. Flat-Faced and Convex-Faced Ceramics [2]

Table 2.1. Characteristics of Alumina Ceramic [2]

Characteristic	Average Value	Standard Deviation
Density (g/cm3)	3.51	0.06
Vickers Microhardness (HV)	386	40
Grain Size (µm)	3	1

Table 2.2. Characteristic of Aluminum Backing Plate [2]

Mechanical Property	Average Value		Standard Deviation	
Tensile Strength (MPa)	244		2	
Total Deformation (%)	19		2	
Rockwell B Hardness[a]	20.0		0.7	
Chemical Composition	**Al**	**Mg**	**Ag**	**Cr**
Element Content (%)[b]	96.7	2.3	0.7	0.2

[a] Using 5 mm steel sphere and 750 g as load.
[b] Estimated by energy-dispersive spectroscopy (EDS).

Schematic diagram of the multi-layered armor system was given in Figure 2.2.

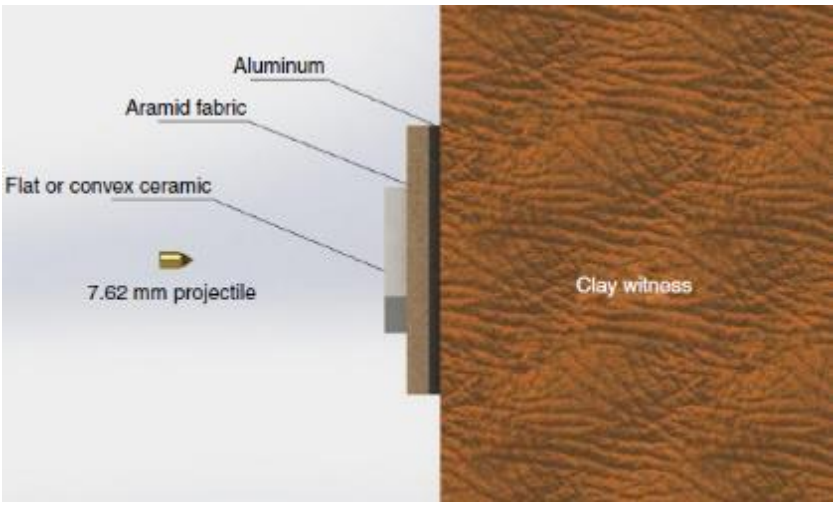

Figure 2.2. Schematic Diagram of the Multi-Layered Armor System [2]

Test results showed that both flat-faced and convex-faced ceramics passed the test according to the NIJ 0101.06 standard for the level III protection. But, back-face signature of the armor was decreased %19 with convex-faced ceramic when compared to flat-faced one. It means that higher energy absorption was observed in convex-faced armor configuration. Test results were given in Table 2.3 [2].

Table 2.3. Ballistic Test Results [2]

Strike Face Geometry	V_i (m/s)	BFS (mm)
Flat	840.45	17.56
	842.78	21.79
	849.90	23.16
	842.07	25.04
	856.16	20.10
	Average: 846 ± 7	Average: 21 ± 3
Convex	853.79	16.5
	846.10	16.3
	844.20	18.3
	Average: 848 ± 5	Average: 17 ± 1

Energy absorption of each layer of composite materials was also investigated in terms of ballistic protection recently. It is found that the fabric layers arranged in front, middle and back of armor panels show different ballistic behavior under ballistic impact. Besides, for a given areal density, hybrid designed armor panels show the best performance when compared to individual woven fabric panels subjected to the ballistic tests [3].

In another research, two types of Twaron fabrics (also called "11F" and "13F") with the same yarns of 93tex and different weave densities, Dyneema uni-directional laminates (also called "U") and clay have been used in ballistic tests. A finite element (FE) model has been formed in order to compare the test results and analysis. A steel projectile with a circular cross-section having 5.5 mm diameter and 1 g mass was used in ballistic tests with average 483 m/s impact velocity value [3].

Specifications of materials are given in Table 2.4 below.

Table 2.4. Specifications of Composite Materials [3]

Material	Code	Yarn Count (tex)		Yarn Density (ends/cm)		Thickness (mm)	Areal Density (g/m^2)
		Warp	Weft	Warp	Weft		
Twaron Fabric	11F	93	93	11	11	0.26	196.85
	13F	93	93	13	13	0.32	251.76
Dyneema UD	U	/	/	/	/	0.24	186.94

Firstly, Twaron fabric panel which is called “11F” was subjected to ballistic test with 1, 15, 24, 36 and 48 layers. Then, hybrid panels were designed according to the test results of the “11F” fabric panel. Schematic diagram of the tests is given in Figure 2.3.

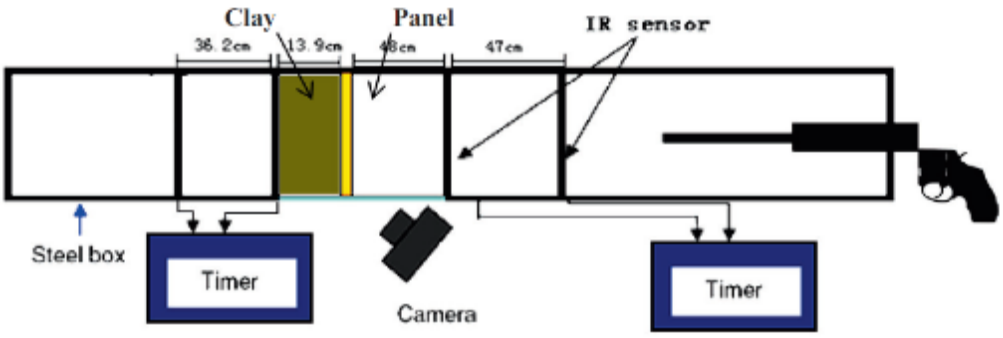

Figure 2.3. Schematic Diagram of the Ballistic Tests [3]

According to the FE model and test results, fabric panel “11F” with 24 layers has stopped the projectile and first seven layers from the front were perforated. It was shown that the last perforated layer (7th layer) had the highest energy absorption then all other front and back layers and energy absorption by each layer was increased from the front layer to the maximum value by the last perforated plate and then started to decrease. Energy absorptions for all 24 layers are given in Figure 2.4 [3].

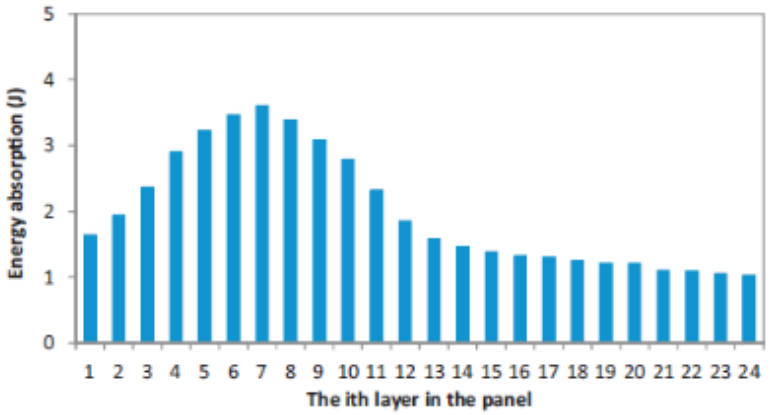

Figure 2.4. Energy Absorption of Each Layer [3]

Based on energy absorption of each layer values, hybrid panels were designed. First 3 layers have been defined as a group one, following 8 layers have been defined as a group two and remaining layers have been defined as a group three according the test results that given in Figure 2.4. By using that classification, two types of hybrid panel design have been

created. In the first design, 3 layers of "13F" fabric panel, 7 layers of "11F" fabric panel and 14 layers of uni-directional laminate have been used. In the second design, 3 layers of "13F" fabric panel, 7 layers of "11F" fabric panel and 5 layers of uni-directional laminate have been used. Test results were given in Table 2.5 [3].

Table 2.5. Test Results [3]

Hybrid Panel	Areal Density (g/m^2)	Impact Velocity (m/s)	Ave Impact Velocity (m/s)	Status	BFS (mm)	Ave BFS (mm)	STD
$11F_{24}$	4724.4	485.04	480.04	Non-Perforated	15.75	15.25	1.12
		473.65		Non-Perforated	13.57		
		482.53		Non-Perforated	14.22		
$13F_3/11F_7/U_{14}$	4750.39	490.25	488.13	Non-Perforated	10.04	10.44	0.87
		487.36		Non-Perforated	11.44		
		486.79		Non-Perforated	9.85		
$11F_{15}$	2952.75	485.04	483.02	Perforated	/	/	/
		481.56		Perforated	/	/	/
		481.06		Perforated	/	/	/
		483.75		Perforated	/	/	/
		487.29		Perforated	/	/	/
		479.41		Perforated	/	/	/
$13F_3/11F_7/U_5$	3067.93	490.70	487.24	Perforated	/	/	/
		487.52		Perforated	/	/	/
		488.25		Perforated	/	/	/
		481.56		Non-Perforated	16.33	15.81	0.61
		489.66		Non-Perforated	15.14		
		485.75		Non-Perforated	15.96		

According to the study, since all results were overlapped with FE model, it is demonstrated that energy absorption of each layer in same fabric type was different. It is also shown that, hybrid designed armor panels show the best performance compared to individual woven fabric panels. It is also observed that, when areal density of armor panel is decreased, projectile could be stopped by hybrid designed panel with more probability than the woven fabric type. These results can be used as guide for hybrid panel design [3].

In general, three type of approaches, namely empirical method, analytical modelling and numerical simulation, are used in order to obtain calculation and validation of armor systems for their impact tests. All approaches have advantages and disadvantages. For example, analytical modelling is used by assuming some hypotheses. Those hypotheses mainly simplify the penetration process. Analytical modelling is one of the fastest way to obtain

solution of projectile-target systems and it can be adapted to the different systems. But, accuracy of analytical modelling is lower than numerical simulation method. Besides, numerical simulation is the only way to get full solution of penetration process. This method consists of solution of the whole differential equations defining the projectile-target system. But, since large CPU time is required, it is hard to obtain results for armor design. Empirical method is the common method for obtain solutions about penetration process. Also, semi-empirical techniques are being developed to match experimental results. This method gives high accuracy but empirical method could be insufficient due to physical phenomena of the penetration process, sometimes like the other approaches [1].

For understanding the multi-layered armor systems, comparisons were performed by using multi-layered armor systems and single layer armor with ballistic tests. For example, by using 7.62 x 51 mm projectile, ballistic tests were performed in order to compare and understand efficient layer quantity of the aramid fiber fabric Kevlar 29 style S745 (plain weave) with areal density of 439 g/m2. In this test, composite panels with 8 layers bonded by neoprene and polyurethane adhesive (for joining panels) were used. Results were compared to multi-layered armor system which includes alumina as a first layer, Kevlar as an intermediate layer and aluminum alloy as a backing plate. Results were also examined by scanning electron microscopy [4].

According to the test results, the projectile was stopped by only using Kevlar fabric with 96 layer. Thickness of 96 layer was equal to 50 mm. It was shown that small thicknesses (up to 20 mm) have limited effect for absorbing energy. Because, according to the microscopy views, up to 20 mm thickness, only few aramid yarns which were in contact with projectile (primary yarns) were deformed. When thickness was increased, other failure modes were observed such as deformation in second yarns and delamination. Test results are given in Figure 2.5 [4].

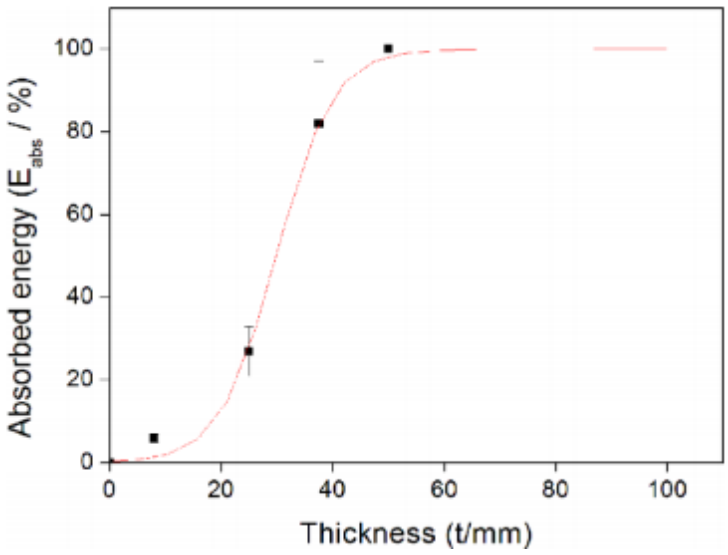

Figure 2.5. Test Results in Terms of Absorbed Energy and Thickness [4]

In contrast, projectile was stopped by only Kevlar fabric of 50 mm thickness. But under the same circumstances, projectile was stopped by multi-layered armor system with a thickness of 25 mm. Thickness of multi-layered armor system was composed of 10 mm of alumina, 10 mm of Kevlar and 5 mm of aluminum alloy. It is shown that using different materials in armor systems show better results both in ballistic performance and lightness. It is determined that, in terms of ballistic performance, different modes of failure need to be obtained during penetration process since front layers of Kevlar fabric have no effect on energy absorption [4].

Recently, experimental and numerical simulations were also performed for one of the high strength aluminum alloy which is 2014-T652. In ballistic tests, both below and above the regions of ballistic limits were tested by variation on velocity values between 800 to 1370 m/s. It is shown that combination of different failure modes were observed in penetration process such as hydrodynamic flow, spalling, ductile hole growth and scabbing. In order to understand quasi-brittle fracture of aluminum alloy, ballistic tests, analytical analysis, dynamic material characterization and numerical simulations were performed. In ballistic tests, steel balls which have 10 mm diameter and 830 HV10 hardness as a projectile and aluminum alloy which has 15 mm thickness as a target were used. Impact and residual velocity values were measured by using high speed camera [5].

Ballistic test results are given below in Table 2.6. According to the test results, splash was observed on the impact face of the target which is caused by compressive shock waves that propagate through projectile and target in all experiments. Spalling on the impact face

of target material was observed due to reflection of the compressive shock waves from the stress-free lateral surfaces of the projectile as tensile rarefaction waves [5].

Table 2.6. Test Results [5]

Shot No	V_i (m/s)	V_r (m/s)
1	803	Not Perforated
2	834	57
3	869	229
4	995	421
5	1166	661
6	1247	786
V_i: Impact Velocity **V_r: Residual Velocity**		

For the material characterization, tensile tests were performed for using the obtained values in models at a different stress tri-axialities, strain rate and temperatures. Johnson-Cook plasticity model was used as a plasticity model. Johnson-Cook failure model and simple tensile pressure failure model were used as a failure model. Also, numerical simulations which represent spherical projectile impacting at a circular target were carried out. Since scabbing was observed in all experiments, Johnson-Cook failure model was insufficient when compared to ballistic test results. It is known that Johnson-Cook failure model was developed for a ductile failure and this model was based on fracture strain. However, much better agreement with test results was attained by using simple tensile pressure failure model which is based on maximum value of hydrostatic tensile stress in a material since quasi-brittle facture was observed during the ballistic tests [5].

Another study was carried out for thickness assessment and statistical optimization for multi-layered armor system consisting of ceramic material, composite material and aluminum alloy recently. In this study, hexagonal alumina which is doped with 4 wt % niobia has been used as a ceramic front layer, non-woven fabric-reinforced curaua used as a composite second layer and 5052 H34 aluminum alloy used as a backing plate in armor configuration. Statistical tools such as the Box-Behnken Design (BBD) and Multiple Regression Analysis (MRA) were used in order to optimize thickness of each layers. Also, ballistic tests were carried out with projectile which is 7.62 x 51 mm NATO commercial with respect to NIJ 0101.06 standard. Schematic diagram of the armor configuration was given in Figure 2.6 [6].

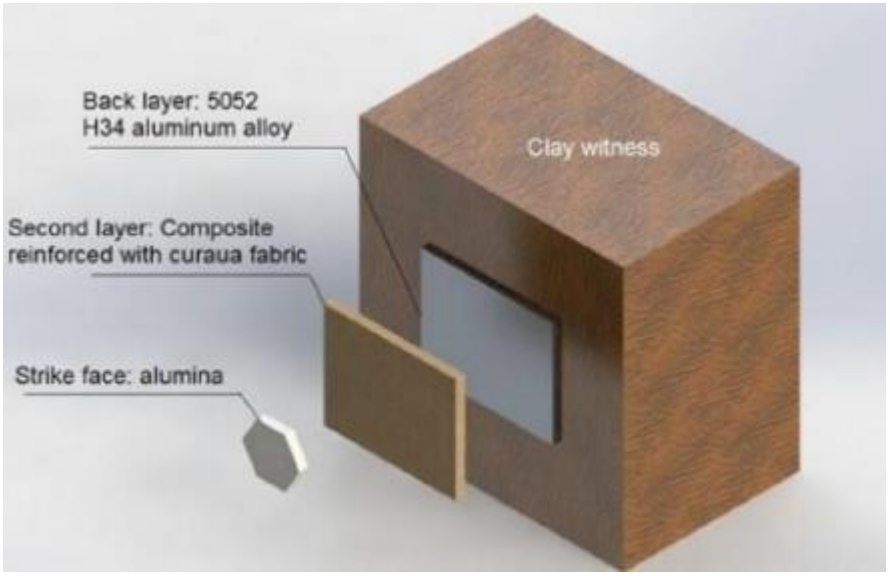

Figure 2.6. Schematic Diagram of the Configuration [6]

Different thickness values were used for each layer in ballistic tests and optimization studies. Every configuration which include different layer thicknesses were labelled. Layer information and ballistic test results were given in Table 2.7 and Table 2.8 [6].

Table 2.7. Layer Information [6]

Layer Information	**Ceramic**		**Fabric Reinforced Composite**		**Aluminum Alloy**	
	t_1 (mm)	**D_{sup} (kg/m^2)**	**t_2 (mm)**	**D_{sup} (kg/m^2)**	**t_3 (mm)**	**D_{sup} (kg/m^2)**
1'	8.5	30.01	6.5	6.96	3.0	7.98
0	10.5	37.07	11.5	12.31	5.0	13.30
1	12.5	44.13	16.5	17.65	7.0	18.62
D_{sup}: Areal density						

Table 2.8. Test Results [6]

BBD Specimen Code	D_{sup} (kg/m^2)	Trauma (mm)
1'1'0	50.5	37/37
11'0	64.6	20/14
1'10	61.2	29/21
110	75.3	21/16
1'01'	50.4	53/42
101'	64.5	22/22
000	62.9	28/28/27
1'01	61.2	20/25
101	75.3	9/21
01'1'	52.1	51/57
011'	62.8	24/35
01'1	62.9	17/25
011	73.9	14/26
000	62.9	22/20/19
D_{sup}: Areal density		

Test results were evaluated in terms of trauma (calculation of back face signature) which was specified 44 mm in the NIJ 0101.06 standard as a limit. According to the optimization studies, aluminum alloy layer showed higher efficiency than the other layers in terms of trauma absorption. It is also shown that, within the range, the best ballistic performance was obtained by using maximum thickness value of ceramic armor and aluminum alloy and minimum thickness value of composite armor. It is also explained that, 8.8% reduction in thickness and 1.3% reduction in the areal density can be observed as a result of both test results and optimization studies in this research [6].

In another study, experiments and numerical simulations were conducted for tungsten alloy rods which are penetrating into multi-layered armor system. In order to evaluate the results, depth of penetration measurements were performed. During the tests and simulations, 125 tungsten alloy long cylindrical rod projectile which has 20° nose cone, 120 mm total length and 5.6 mm diameter with 17.54 g/m3 tungsten alloy density were used. In multi-layered armor system, alumina ceramic armor which has 100 mm in thickness used as a first layer and 603 armor steel which has 150 mm diameter and 80 mm thickness used as a backing plate. Different thickness and boundary conditions were used for ceramic armor which was placed in first layer. During the tests, the impact velocity of the projectile was measured approximately 1600 m/s which is relatively high. A single layer which is 603 armor steel were exposed to the ballistic test. The aim of this study was to explain

relationships between ceramic thicknesses and residual penetration depth/mass efficiency factor/differential efficiency factor. On the other hand, ballistic performance was also measured with different boundary conditions such as with lateral constraint and without lateral constraint. Schematic diagram of the ballistic test was given in Figure 2.7 [7].

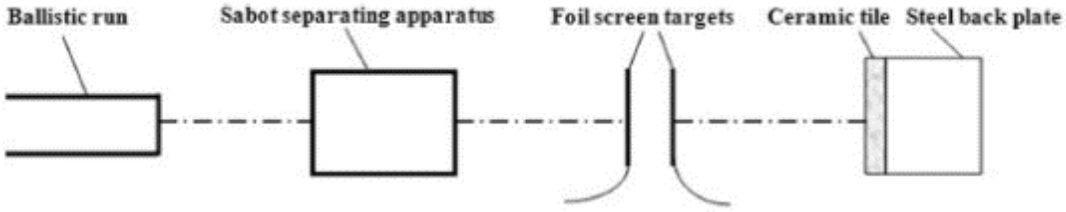

Figure 2.7. Schematic Diagram of the Ballistic Tests [7]

Ballistic launcher which was 20 mm and foil screen target measuring system for measuring initial velocity of the gun bore were used in tests. It is noticed that ceramic armor which was directly behind the impact location, was completely damaged and failed. Test results were given in Table 2.9 where Pt is the residual penetration depth acquired from ballistic tests, Ps is the residual penetration depth acquired from numerical simulations [7].

Table 2.9. Test (with Barrel Holder) and Simulation Results [7]

Shot Number	Ceramic Thickness (mm)	Velocity (m/s)	P_t (mm)	P_s (mm)	$\Delta P=\|P_s-P_t\|$ (mm)	$\Delta P/P$ (%)
1-1	0	1664	96	96	-	-
1-2	30	1611	73	78.1	5.1	5.3%
1-3	30	1600	72	71.5	0.5	0.52%
1-4	50	1577	55	56	1	1.0%
1-5	70	1554	35	32.6	2.4	2.5%
1-6	70	1577	33	38.0	5.0	5.2%
1-7	90	1575	10	13.7	3.7	3.9%

Johnson and Holmquist 2 model for ceramic material and Johnson and Cook constitutive model and Mie-Grüneisen models for steel materials and projectile were used in numerical simulations. According to the comparison in Table 2.9, numerical simulation and test results were overlapped in terms of residual depth penetration with less than 6% error. It is shown that, when ceramic thickness increases, ballistic performance of the multi-layered armor system increases almost linearly. Test results which were performed without barrel holder are given in Table 2.10 [7].

Table 2.10. Test Results without Barrel Holder [7]

Simulation Number	Ceramic Thickness (mm)	Velocity (m/s)	P_s (mm)	Mass Efficiency Factor	Differential Efficiency Factor
2-1	30	1611	78.1	1.130	1.742
2-2	50	1577	56.0	1.147	1.497
2-3	70	1554	38.0	1.180	1.421
2-4	90	1577	13.7	1.600	1.807
2-5	20	1664	79.7	1.009	1.090
2-6	40	1664	67.0	1.034	1.160
2-7	60	1664	50.1	1.147	1.413
2-8	80	1664	34.7	1.257	1.496
2-9	100	1664	5.4	1.615	1.737
2-10	110	1664	0	/	/

Comparing the test results given in Table 2.9 and Table 2.10, it can be seen that ballistic performance of the multi-layered armor system with constrained configuration was better than unconstrained configuration because of the lateral rarefaction wave that reflected from the boundary. It can also be noted that when residual penetration depth decreases, mass efficiency factor which can be calculated by Yaziv formula and differential efficiency factor which can calculated by Yaziv and Rosenberg formula increases respectively. Finally, it can be noted that, by increasing ceramic tile thickness values, depth of penetration decreases, on the other hand, mass efficiency and differential efficiency factor increases which means better ballistic performance of overall multi-layered armor system [7].

Ballistic performance of the multi-layered armors systems which include aligned fibers and fabric of fique fibers as a composite armor with two configurations were investigated in another study. Both fique fabric and aligned fibers with 10 vol.%, 20 vol.% and 30 vol.% were used for reinforcement of polyester matrix composite. Different type of the composite materials used in experiments were given in Figure 2.8 [8].

Figure 2.8. Aligned Fibers and Plain Weave Fabric [8]

In the ballistic tests, alumina which has a thickness of 10 mm was used as a first layer, polyester composite that reinforced with configurations of fique fiber which has 10 mm thickness was used as a second layer and 5052 H34 aluminum alloy which has 5 mm thickness was used as a backing plate. The layers were bonded by using polyurethane adhesive. All composite material samples for ballistic tests were prepared by compression molding in the amounts of 10 vol.%, 20 vol.% and 30 vol.% of intermediate material layer. 7.62 x 51 mm NATO commercial projectile was used in ballistic tests with respect to NIJ 0101.06 standard. Results were evaluated in terms of back-face signature (also called indentation depth) and these results were compared with another multi-layered armor configuration that has aramid fabric laminate as an only difference. Test results were given in Table 2.11 [8].

Table 2.11. Test Results [8]

Fique Fiber	**Intermediate Material Layer**	**Average Depth of Indentation (mm)**
Aligned	30 vol.%	17 ± 2
	20 vol.%	16 ± 1
	10 vol.%	17 ± 3
Fabric	30 vol.%	20 ± 2
	20 vol.%	17 ± 3
	10 vol.%	16 ± 3
	Aramid Fabric Laminates	23 ± 3

According to the test results, perforation was not observed in any configuration which include aligned fibers and fabric with different volumes. On the other hand, ceramic armor layers (first layers) were destructed in all configurations. Different failure modes such as rupture of the polyester matrix, delamination and individual rupture of fique fibers were observed. It is noted that rupture of the polyester matrix was the main failure mode for the aligned fibers. It is also noted that, fique fiber variations were showed better ballistic performance when compared with aramid fabric laminates. Besides, back face signature values for fique fiber variations were nearly same and below the limit which is 44 mm that described in NIJ 0101.06 standard. It was noticed that, only fique fabric composites were able to keep their integrity after ballistic impact and it means, they could provide protection against the multi-hit shooting [8].

In another study, hardness of the steel which were used as a front layer and backing plate, on ceramic armor was investigated. Both experimental studies and numerical simulations were carried out. In the tests, AISI 4340 steel with 5 mm thickness was used as front covers

of configurations with different hardness values, silicon carbide with 20 mm thickness was used as a second layer, AISI 4340 steel with 10 mm thickness was used as a backing plate of configurations with different hardness values and AISI 4340 steel with 80 mm thickness and 30 HRC values was used as a witness block for evaluation of the test results. Silicon carbide was bonded to the backing plate with epoxy adhesive which is Loctite NA3909.3 with 0.5 mm thickness in all configurations. Also, cover plate was attached to the system with M8 screws at the 4 corners in all configurations. There was an air gap with 75 mm between backing plate and witness block. Hardness values which are 30 HRC, 40 HRC and 50 HRC were used both in cover plate and backing plate in all individual ballistic impact tests and the areal density of the multi-layered armor system was fixed at 180 kg/m2. W4Ni3Fe tungsten alloy with mass of 96 g and L/D ratio of 13.8 was used as a projectile with 1.25 km/s velocity in the tests. Firstly, depth of penetration tests were performed in order to determination of relationship between depth of penetration and velocity. AISI 4340 steel with thickness of 120 mm was used for the depth of penetration tests. Depth of penetration test results and determined relationship equation are given in Figure 2.9 [9].

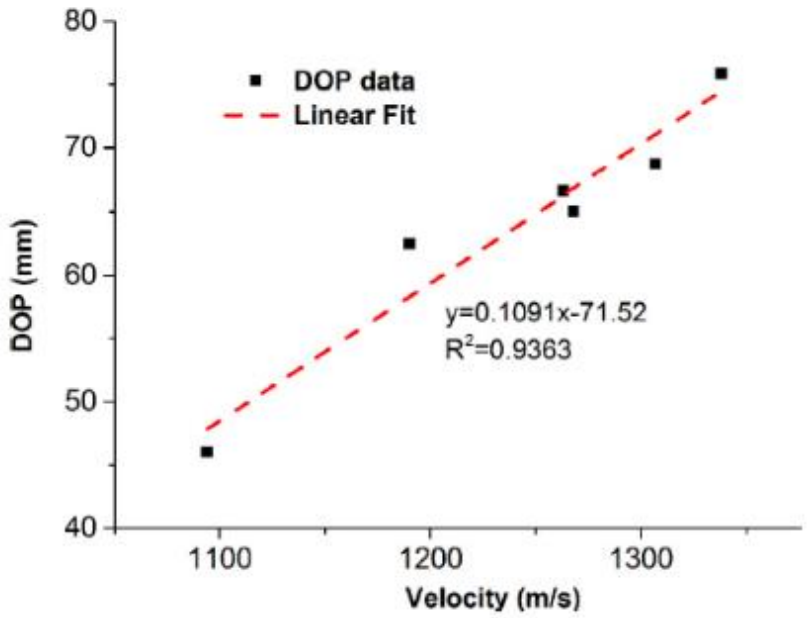

Figure 2.9. Test Results of Depth of Penetration Tests [9]

Properties of the materials are given in Table 2.12 [9].

Table 2.12. Material Properties [9]

Materials	ρ_0 (kg/m^3)	E (GPA)	Yield Strength (MPa)	Ultimate Tensile Strength (MPa)	Vickers Hardness (kgf/mm^2)
4340 (HRC 30)	7850	210	850 ± 59	1020 ± 37	298 ± 7
4340 (HRC 40)	7850	210	1212 ± 4	1376 ± 3	412 ± 6
4340 (HRC 50)	7850	210	1424 ± 9	1713 ± 7	510 ± 3
Tungsten Alloy	17.600	320	636 ± 11	902 ± 9	260 ± 10
Grade F Plus SiC	3190	430	-	-	2450 ± 130

Schematic diagram of the ballistic test was given in Figure 2.10 [9].

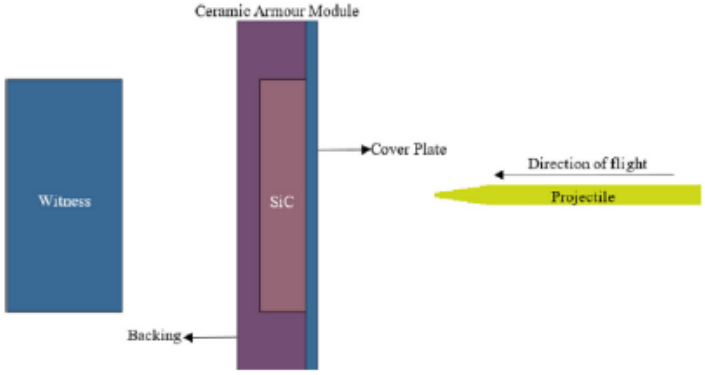

Figure 2.10. Schematic Diagram of the Ballistic Tests [9]

Ballistic test results which were performed by using different hardness backing plates are given in Table 2.13. Mean reference depth of penetration values were calculated by using the equation which was given on Figure 2.9 [9].

Table 2.13. Ballistic Test Results with Different Hardness of Backing Plates [9]

S/N	Hardness (HRC)	Velocity (m/s)	Mean Reference DOP (mm)	Mean Residual DOP (mm)
B30-1	30	1244	64.2	27.0
B30-2	30	1244	64.2	27.0
B30-3	30	1286	68.8	30.0
B40-1	40	1263	66.3	27.0
B40-2	40	1256	65.5	19.0
B40-3	40	1256	65.5	19.5
B50-1	50	1229	62.6	11.5
B50-2	50	1246	62.7	10.0
B50-3	50	1235	64.4	12.8

According to the test results, it can be seen that when hardness values of the backing plate increased, ballistic performance of the multi-layered armor systems also increased accordingly for the thickness value of 10 mm [9].

Ballistic test results which were performed by using different hardness of front cover plates were given in Table 2.14 [9].

Table 2.14. Ballistic Test Results with Different Hardness of Front Covers [9]

S/N	Hardness (HRC)	Velocity (m/s)	Mean Reference DOP (mm)	Mean Residual DOP (mm)
C30-1	30	1195	58.9	14.0
C30-2	30	1269	66.9	16.3
C30-3	30	1239	63.7	19.7
C40-1	40	1247	64.5	15.9
C40-2	40	1247	64.5	18.3
C40-3	40	1237	63.4	16.9
C50-1	50	1233	63.0	15.9
C50-2	50	1293	69.6	27.5
C50-3	50	1220	61.6	12.6

According to the test results, it can be seen that increasing hardness values of the front cover has no effect on the ballistic performance of the multi-layered armor system for the thickness value of 5 mm. But, it was also noticed that, in another study by performing ballistic tests with the front cover with the thickness of 25 mm, it was reported that when hardness values of the front cover increased, ballistic performance of the multi-layered armor systems also increased accordingly [9].

Numerical simulations were carried out by using Johnson and Cook model for tungsten alloy and AISI 4340 steel and Johnson and Holmquist – 1 model for silicon carbide. Good agreement between numerical simulations and ballistic test results were obtained. Comparison results with respect to mass efficiency are given in Figure 2.11 [9].

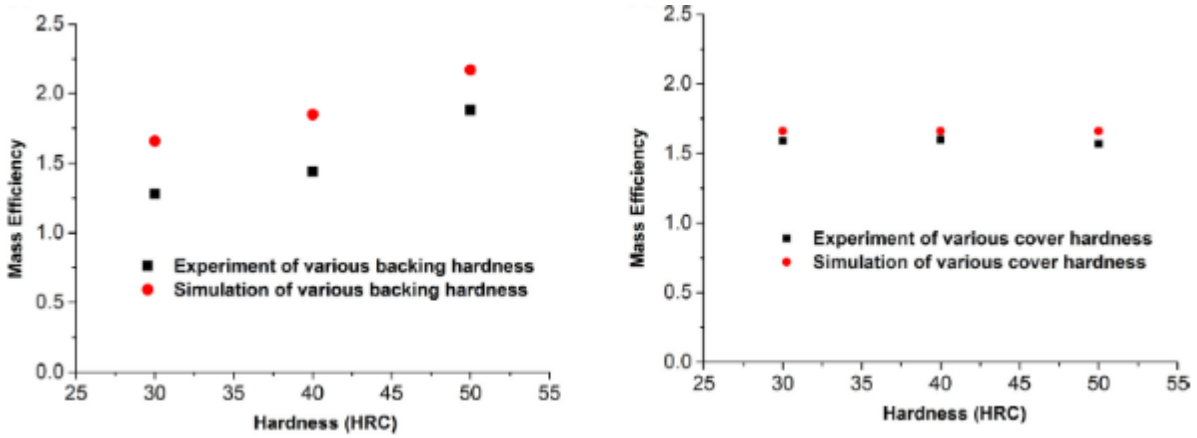

Figure 2.11. Comparison Results Between Numerical Simulations and Ballistic Tests [9]

To understand the effect of the hardness values of backing plate, simulation results are given in Figure 2.12 [9].

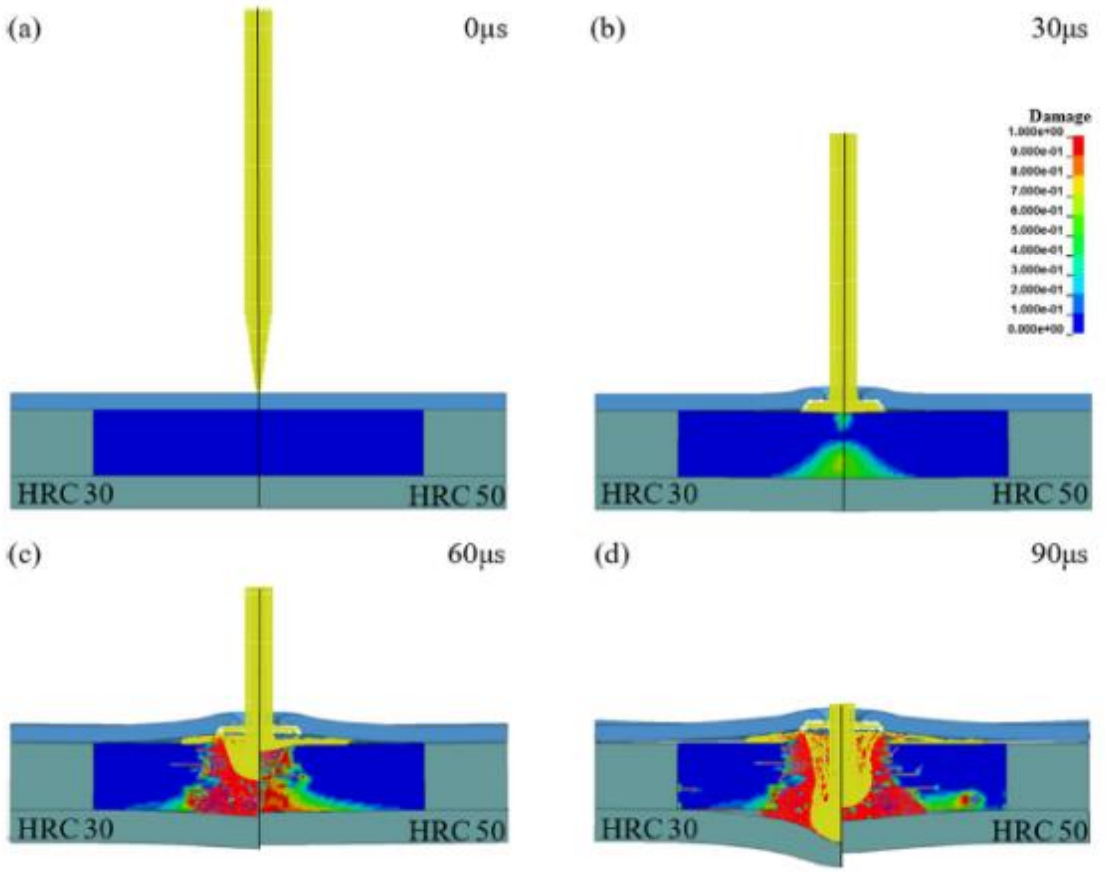

Figure 2.12. Results and Comparisons of the Numerical Simulations with respect to 30 HRC and 50 HRC Hardness Values of the Backing Plates at Different Times of Penetration Process (a) 0 μs, (b) 30 μs, (c) 60 μs and (d) 90 μs [9]

Hardness of the backing plate has effect on dwell time. Longer dwell time on the ceramic armor means more erosion in projectile, therefore, better ballistic performance can be obtained that can be seen from Figure 2.12. It can also noted that, thin cover plates such as thickness of 5 mm have no effect on ballistic performance of the multi-layered armor systems while cover plate thickness of 25 mm have significant effect [9].

Impact of 7.62 mm armor piercing projectile into 5083 aluminum armors also investigated recently. Numerical simulations and ballistic tests were carried out in order to understand penetration mechanism. 5083 series aluminum armors with the thickness of 25 mm and 32 mm were used in ballistic tests and numerical simulations. P80 projectiles with 9.75 g mass were used as projectiles in ballistic tests. Impact velocities were set to 864 ± 6 m/s and residual velocities were measured. In this study, failure mechanism of both projectile and target, effects of the parts of projectile and estimated thickness for not perforation case were tried to investigate. Cross sectional image of the projectile is given in Figure 2.13 [10].

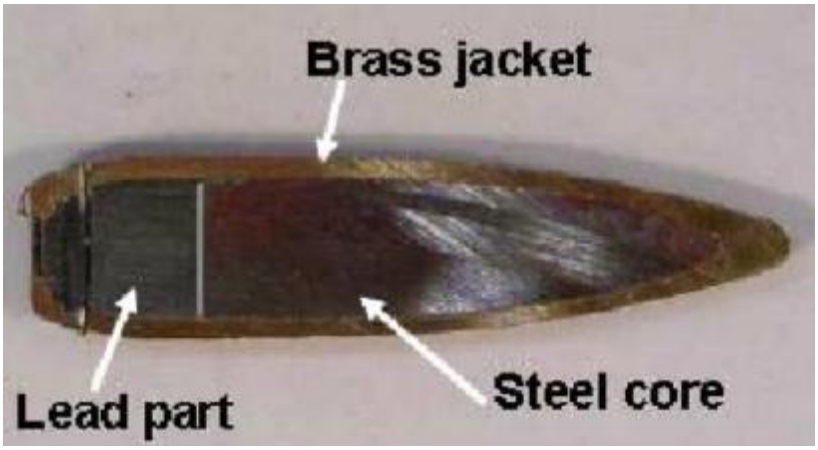

Figure 2.13. Cross Section of the P80 Projectile [10]

According to the test results, residual velocity of the projectile was measured around 673 ± 10 m/s for the thickness of 25 mm of 5083 aluminum armor. It was also observed that, ductile hole growth and petaling in the entrance and exit points of the projectile were the failure mechanism of the aluminum armor. Petaling that occurred in the entrance and exit points were shown in Figure 2.14 [10].

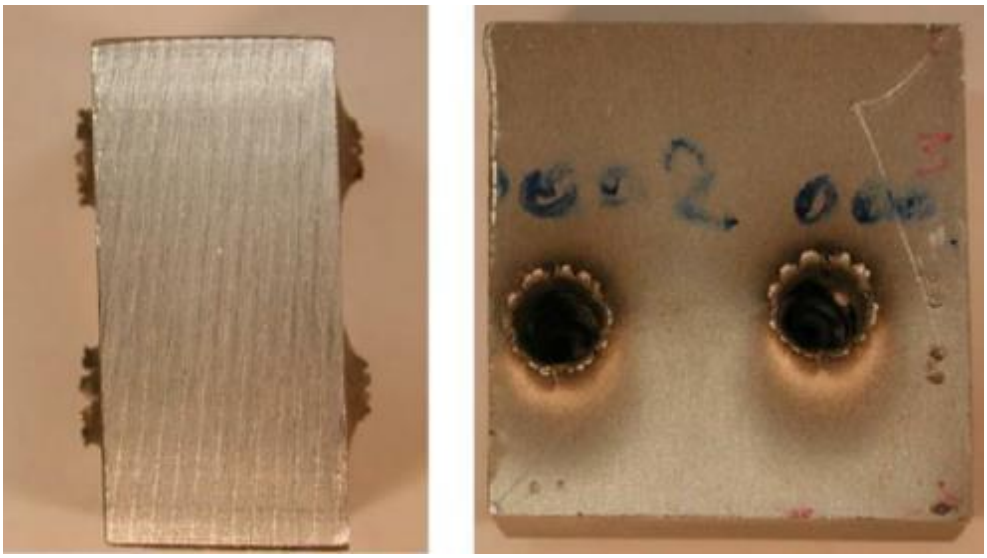

Figure 2.14. Petaling in the Entrance and Exit Points [10]

It was noticed that, brass jacket of the projectile was kept by the armor in the middle of penetration channel. Because of that, two different size holes were observed in cross section of the armor. Hole diameter which is larger than projectile diameter was seen on channel 1 because of the brass jacket of the projectile. In the second channel, hole diameter was equal to steel core diameter of the projectile. It was noted that, steel core of the projectile was not fractured and/or deformed. Cross section of the armor was given in Figure 2.15 [10].

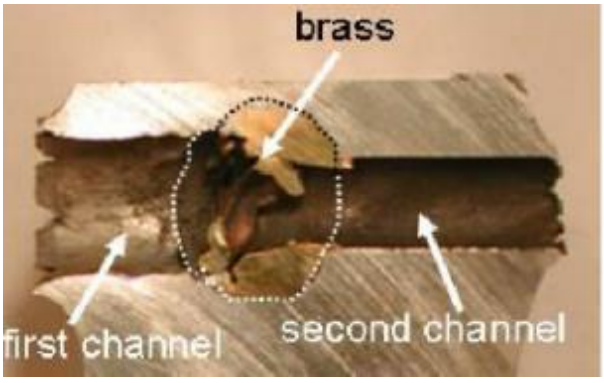

Figure 2.15. Cross Section of the Armor [10]

As a result, failure mechanisms and the penetration process were explained in this study. It is also noted that, good agreement between numerical simulations and test results were observed. Minimum thickness of armor for not perforation case was found 50 mm with only 5% error compared with test results that carried on another study. Effects of lead core and jacket for the projectile were compared and it was seen that jacket increased the power of

penetration slightly compared with without jacket projectile. It was also observed that lead core had a greater contribution to the both penetration and perforation processes [10].

The effects of the using interlayers in multi-layered armor systems are also being investigated. Recently, usage of EPDM rubber, Teflon and aluminum foam interlayers in multi-layered armor systems were studied. Numerical simulations and ballistic tests were carried out in this research. In configurations, alumina with interlayer and without interlayer were used as a front layer and plain wave S2 glass fabric was used as a backing plate. It means rubber, teflon and aluminum foam interlayers were inserted between alumina and glass fabric layers. The thicknesses of 1.5 mm, 2 mm and 18 mm were used for each interlayers. Ballistic test were carried out with 7.62 x 51 mm M61 type armor piercing projectile with 800 ± 10 m/s velocity values [11].

According to the numerical simulation results, it was shown that, teflon and aluminum foam interlayers were the cause of significant delay in the initial stress build-up in the composite layer. It was also seen that, magnitude of the stress that was transmitted to composite backing plate was lower than without interlayer and EPDM rubber configurations. According to the test results, relatively large pieces of ceramic tile were fragmented in without interlayer and EPDM rubber configurations. It means, using teflon and aluminum foam interlayers helped to spread the damage zone in the radial direction. These results were overlapped with numerical simulations. Numerical results are given in Figure 2.16 and Figure 2.17 [11].

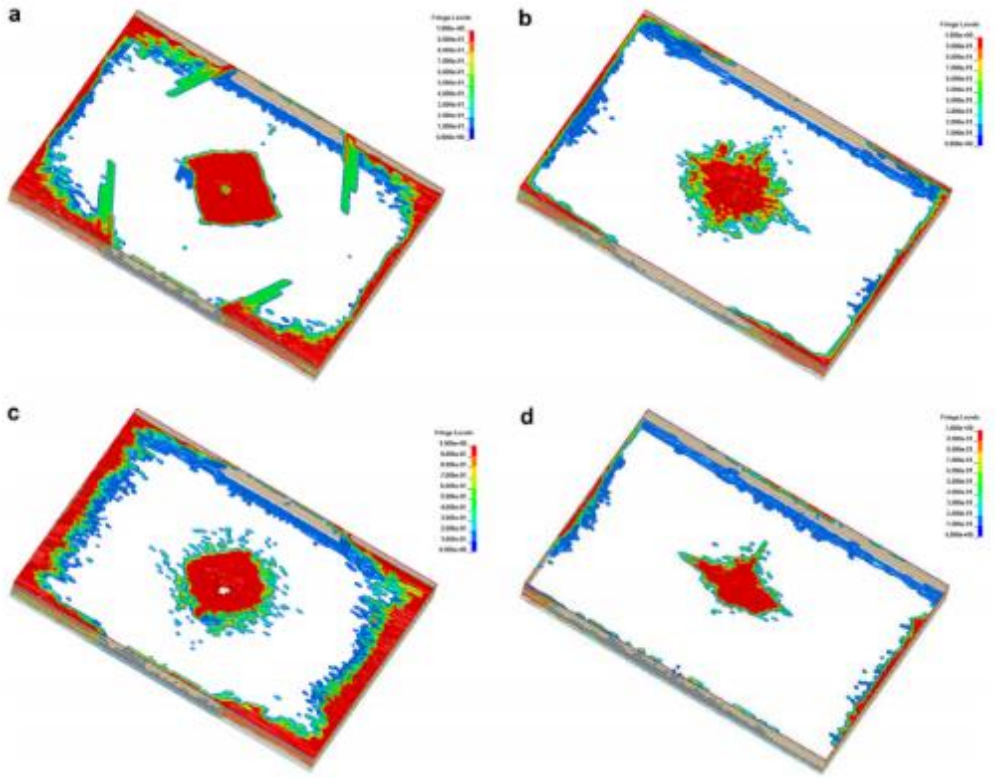

Figure 2.16. Delamination Contours in the Composite Layers after 250 μs of Impact (a) without Interlayer, (b) EPDM Rubber Interlayer, (c) Teflon Interlayer and (d) Aluminum Foam Interlayer Configurations [11]

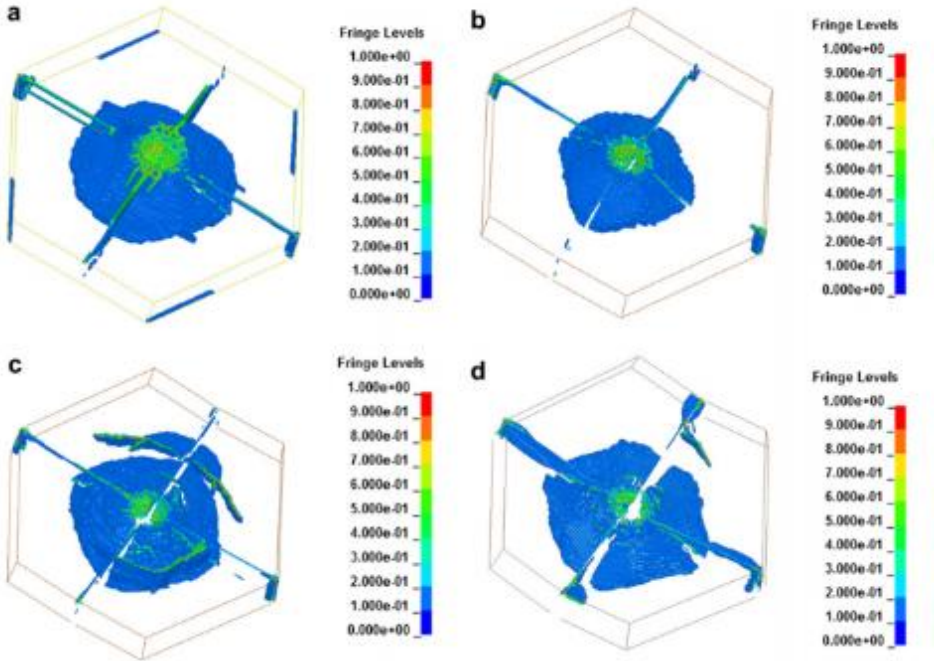

Figure 2.17. Damage Contours in the Ceramic Layers after 250 μs of Impact (a) without Interlayer, (b) EPDM Rubber Interlayer, (c) Teflon Interlayer and (d) Aluminum Foam Interlayer Configurations [11]

3. ANALYTICAL MODELS FOR ARMOR SYSTEMS

Multi-layer armor systems have emerged as a result of the use of steel, aluminum, composite and ceramic materials in armor systems with different configurations. By combining the physical and therefore ballistic properties of different materials, optimum ballistic performances with low areal densities are obtained. Various configurations created within the scope of different studies have been subjected to a series of tests, and quasi-experimental analytical models have been put forward with reference to the results of these tests. These analytical models, which were created, were used many times in subsequent studies and verified over and over again, and analytical models that give the most accurate results depending on the relevant armor configuration have been continuously developed and continue to be developed.

3.1. Pol Model

In 2009, a theoretical model for calculation of ballistic limit of thin metallic layer (such as steel and aluminum) was improved by Pol, Bidi, Hoseini and Liaghat [12]. Failure mode was accepted as a asymmetry petalling in this model and the basis of this model was equality of the work done and energy balance. Several ballistic tests were carried out by Pol and his friends and this model was verified by comparing the test results and analytical calculations. According to this model [12]:

$$V_b = \left(\frac{2W}{M}\right)^{\frac{1}{2}} \quad (1)$$

where:

V_b is stands for ballistic limit of the metallic layer,

W is stands for total work done,

M is stands for projectile mass.

W which is stands for total work done calculated as follows:

$$W = W_p + W_d + W_b \quad (2)$$

where:

W_p is stands for work done in plastic deformation,

W_d is stands for dynamic work done,

W_b is stands for dynamic work done in bending of perfect plastic beam.

W_p which is stands for work done in plastic deformation calculated as follows:

$$W_p = \frac{\pi}{2} b^2 Y h_0 \tag{3}$$

where:

b is stands for radius of projectile,

Y is stands for yield strength of the material,

h_0 is stands for thickness of material.

W_d which is stands for dynamic work done calculated as follows:

$$W_d = \frac{2\pi\rho V_0^2 b^4 h_0^2}{3L^2} \tag{4}$$

where:

ρ is stands for density of armor plate,

V_0 is stands for impact velocity,

L is stands for nose length of projectile.

W_b which is stands for dynamic work done in bending of perfect plastic beam calculated as follows:

$$W_b = \frac{\pi^2 b h_0^2 Y}{4} \tag{5}$$

3.2. Lambert - Jonas Model

In 1976, a mathematical model was improved focused on relationship between striking and residual velocity in terms of ballistic testing. This model allows calculation of residual velocity of the projectile which completely penetrate the metallic layers. Several ballistic tests were carried out by Lambert and Jonas and this model was verified by comparing the test results and mathematical calculations. According to this model [13]:

$$V_r = a(V_s^P - V_l^P)^{\frac{1}{P}} \tag{6}$$

where:

V_r is stands for residual velocity,

a is stands for parameter from the regression procedure,

V_s is stands for striking velocity,

P is stands for experimental constant,

V_l is stands for ballistic limit of target.

a which is stands for parameter from the regression procedure calculated as follows:

$$a = \frac{m_p}{m_p + m^I} \tag{7}$$

where:

m_p is stands for mass of projectile,

m^I is stands for mass of the area of armors which is deformed during penetration.

m^I which is stands for mass of the area of armors which is deformed during penetration calculated as follows:

$$m^I = \pi r^2 \rho_t h_t \tag{8}$$

where:

r is stands for radius of projectile,

ρ_t is stands for density of target,

h_t is stands for thickness of target.

P which is stands for experimental constant calculated as follows:

$$P = 2 + \frac{z}{3} \tag{9}$$

where:

z is stands for constant value.

z which is stands for constant value calculated as follows:

$$z = \frac{h_t}{d} \sec(\beta)^{0.75} \tag{10}$$

where:

d is stands for diameter of projectile.

3.3. Tang and Wen Model

In 2016, a formula was improved focused on energy dissipation of both projectile and ballistic layers. This model also allows calculation of residual velocity of projectile which left the ceramic layer. Several ballistic tests were carried out for this model and model was verified by comparing the test results and analytical calculations. According to this model [14]:

$$v_s = \sqrt{\frac{2E_{kb}}{m_r}} \tag{11}$$

where:

v_s is stands for speed of the residual projectile when it impacts the backing plate,

E_{kb} is stands for the kinetic energy of the residual projectile,

m_r is stands for the mass of the residual projectile.

E_{kb} which is stands for the kinetic energy of the residual projectile calculated as follows:

$$E_{kb} = E_k - E_p - E_c \tag{12}$$

where:

E_k is stands for the initial kinetic energy of the projectile,

E_p is stands for the kinetic energy loss of the projectile when it impacts the ceramic tile,

E_c is stands for the energy dissipation of the ceramic facing.

E_k which is stands for the initial kinetic energy of the projectile calculated as follows:

$$E_k = \frac{1}{2} m_p v_0^2 \tag{13}$$

where:

m_p is stands for the mass of the projectile,

v_0 is stands for the impact velocity.

E_p which is stands for the kinetic energy loss of the projectile when it impacts the ceramic tile calculated as follows:

$$E_p = \pi d_0^2 Y_p l_e / 4 \tag{14}$$

where:

d_0 is stands for the initial diameter of the projectile,

Y_p is stands for the dynamic yield strength of the projectile,

l_e is stands for the erosion length of the projectile.

l_e which is stands for the erosion length of the projectile calculated as follows:

$$\frac{l_e}{d_0} = \zeta\left(\frac{HEL v_0 h_{c0} \sqrt{\frac{\rho_p}{Y_p^3}}}{d_0}\right) \tag{15}$$

where:

ζ is stands for the empirical constant which can be determined from experiments,

HEL is stands for Hugoniot elastic limit of ceramic,

h_{c0} is stands for the initial thickness of the ceramic,

ρ_p is stands for the density of the projectile.

E_c which is stands for the energy dissipation of the ceramic facing calculated as follows:

$$E_c = E_{cs} + E_{cc} \tag{16}$$

where:

E_{cs} is stands for the energy dissipated by shear in ceramic facing,

E_{cc} is stands for the energy dissipated by crushing in ceramic facing.

E_{cs} which is stands for the energy dissipated by shear in ceramic facing calculated as follows:

$$E_{cs} = \begin{cases} \pi\tau_s\left(\frac{d_p h_{c0}^2}{2} + h_{c0}^3 \tan\frac{\theta}{3}\right)/(\cos\theta)^2 & for\ h_{c0} \le h_c \\ \pi\tau_s\left(\frac{d_p h_c^2}{2} + h_c^3 \tan\frac{\theta}{3}\right)/(\cos\theta)^2 & for\ h_{c0} > h_c \end{cases} \tag{17}$$

where:

τ_s is stands for the shear strength of the ceramic,

d_p is stands for the diameter of projectile after deformation/mushrooming,

θ is stands for semi-angle of ceramic cone,

h_c is stands for the critical thickness of the ceramic plate between shear and compress.

d_p which is stands for the diameter of projectile after deformation/mushrooming calculated as follows:

$$d_p = k_1 d_0 \tag{18}$$

where:

k_1 is stands for the ratio of projectile deformed diameter to its initial diameter,

d_0 is stands for the initial diameter of projectile.

k_1 which is stands for the ratio of projectile deformed diameter to its initial diameter calculated as follows:

$$k_1 = (1 - \delta)^{-1/2} \tag{19}$$

where:

δ is stands for the reduction of cross-section area.

θ which is stands for the semi-angle of ceramic cone calculated as follows:

$$\theta = \left(\frac{v_0 - 220}{780}\right)\frac{34\pi}{180} + \frac{34\pi}{180} \tag{20}$$

h_c which is stands for the critical thickness of the ceramic plate between shear and compress calculated as follows:

$$h_c = \frac{\left[-d_p + \sqrt{d_p^2 + 4F_{cc}\sin\theta}\right]}{2\tan\theta} \tag{21}$$

where:

F_{cc} is stands for the maximum compressive force resistive to the projectile motion.

F_{cc} which is stands for the maximum compressive force resistive to the projectile motion calculated as follows:

$$F_{cc} = \pi\frac{d_p^2}{4}\left[\tau_s\left(\frac{3}{2}\pi + 1\right) + \beta_p\sqrt{2\rho_c\tau_s}u\sin(\frac{\pi}{4})\right] \tag{22}$$

where:

β_p is stands for the empirical constant,

ρ_c is stands for the density of the ceramic facing plate,

u is stands for the penetration velocity of projectile.

u which is stands for the penetration velocity of projectile calculated as follows:

$$u = k_2 v_0 \tag{23}$$

where:

k_2 is stands for the ratio of penetration velocity to initial velocity.

E_{cc} which is stands for the energy dissipated by crushing in ceramic facing calculated as follows:

$$E_{cc} = F_{cc} h_{c0} \tag{24}$$

m_r which is stands for the mass of the residual projectile calculated as follows:

$$m_r = m_p - \frac{\pi d_0^2 \rho_p l_e}{4} \tag{25}$$

4. EXPERIMENTAL STUDIES

Ballistic tests which were carried out within the scope of experimental studies were performed in an accredited defense industry company ballistic laboratory, following the rules of STANAG 4569 standard. Each configuration was tested once, and 2 shots were fired at each configuration for each test. What makes this study different is that unlike the other studies in the literature, 2 ceramic layers are used one after the other in tested configurations. Because, generally only one layer of ceramic was used in literature. The materials which were used in the test configurations were procured from suppliers of defense industry companies. The materials used in the configurations and the supplier information are given in Table 4.1.

Table 4.1. Material Information

Material	**Thickness (mm)**	**Supplier**
Alumina	10	Nurol Teknoloji
Silicon Carbide	10	Nurol Teknoloji
Steel (MIL-DTL-12560 CL 4A Armox 440T)	4	SSAB
Aluminum (5059-H136, MIL-DTL-46027)	13	Aleris International
Polyurea Coating	≈ 1	Nurol Teknoloji

The layout of the ballistics laboratory where ballistic tests were carried out is shown in Figure 4.1.

Figure 4.1. Layout of Test Laboratory for Ballistic Impact Tests

The detailed information of the Trial Configuration – 1 is shown on Table 4.2, and the physical representation of the Trial Configuration – 1 is shown on Figure 4.2:

Table 4.2. Schematic Diagram of Trial Configuration – 1

Trial Configuration – 1			
Front Layer	**Ceramic Core – 1**	**Ceramic Core – 2**	**Back Plate**
Steel Armor 150 x 150 mm 4 mm thickness	Silicon Carbide[1] 100 x 100 mm 10 mm thickness	Alumina 100 x 100 mm 10 mm thickness	Aluminum Armor 150 x 150 mm 13 mm thickness

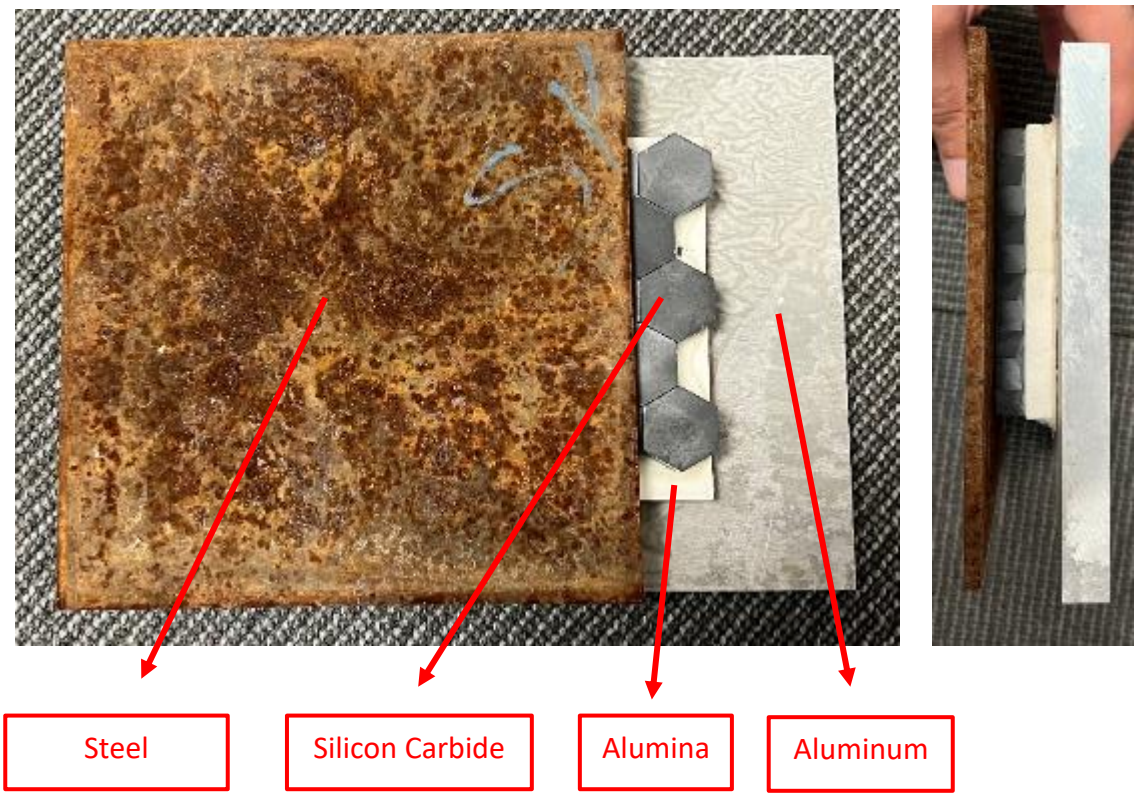

Figure 4.2. Physical Visual of Trial Configuration – 1

The detailed information of the Trial Configuration – 2 is shown on Table 4.3, and the physical representation of the Trial Configuration – 2 is shown on Figure 4.3:

Table 4.3. Schematic Diagram of Trial Configuration – 2

Trial Configuration – 2			
Front Layer	**Ceramic Core – 1**	**Ceramic Core – 2**	**Back Plate**
Polyurea Coating ≈ 1 mm thickness	Silicon Carbide[1] 100 x 100 mm 10 mm thickness	Alumina 100 x 100 mm 10 mm thickness	Aluminum Armor 150 x 150 mm 13 mm thickness

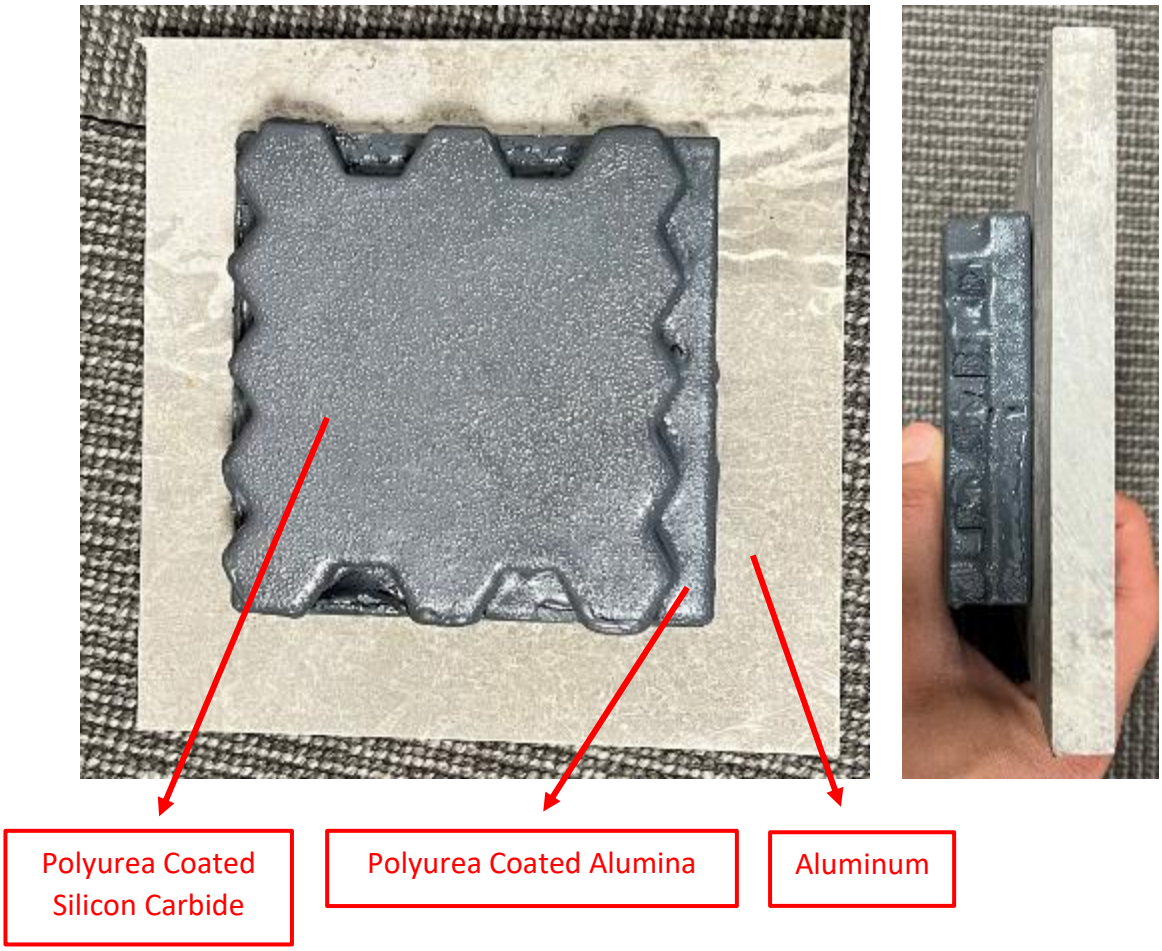

Figure 4.3. Physical Visual of Trial Configuration – 2

[1]10 mm x 10 mm hexagon tiles (total 23 ea) were used only in Trial Configuration – 1 & 2.

Trial Configuration – 1 and Trial Configuration – 2 were used for detection of STANAG 4569 level and proper impact velocity. By using of the data obtained from the trial configurations, ballistic tests were performed according to STANAG 4569 level 3 for the main configurations.

The detailed information of the Configuration – 3 is shown on Table 4.4, and the physical representation of the Configuration – 3 is shown on Figure 4.4:

Table 4.4. Schematic Diagram of Configuration – 3

Configuration – 3			
Front Layer	**Ceramic Core – 1**	**Ceramic Core – 2**	**Back Plate**
Steel Armor 150 x 150 mm 4 mm thickness	Silicon Carbide[2] 100 x 100 mm 10 mm thickness	Alumina[3] 100 x 100 mm 10 mm thickness	Aluminum Armor 150 x 150 mm 13 mm thickness

Figure 4.4. Physical Visual of Configuration – 3

In Configuration – 3, steel layer used as a preliminary layer and ballistic performance effect of the use of steel front layer has been tried to be examined. Silicon carbide layer used as a first ceramic layer and the ballistic performance effect of the sequencing of the alumina and silicon carbide layers has been investigated.

The detailed information of the Configuration – 4 is shown on Table 4.5, and the physical representation of the Configuration – 4 is shown on Figure 4.5:

Table 4.5. Schematic Diagram of Configuration – 4

Configuration – 4			
Front Layer	**Ceramic Core – 1**	**Ceramic Core – 2**	**Back Plate**
Polyurea Coating ≈ 1 mm thickness	Silicon Carbide[2] 100 x 100 mm 10 mm thickness	Alumina[3] 100 x 100 mm 10 mm thickness	Aluminum Armor 150 x 150 mm 13 mm thickness

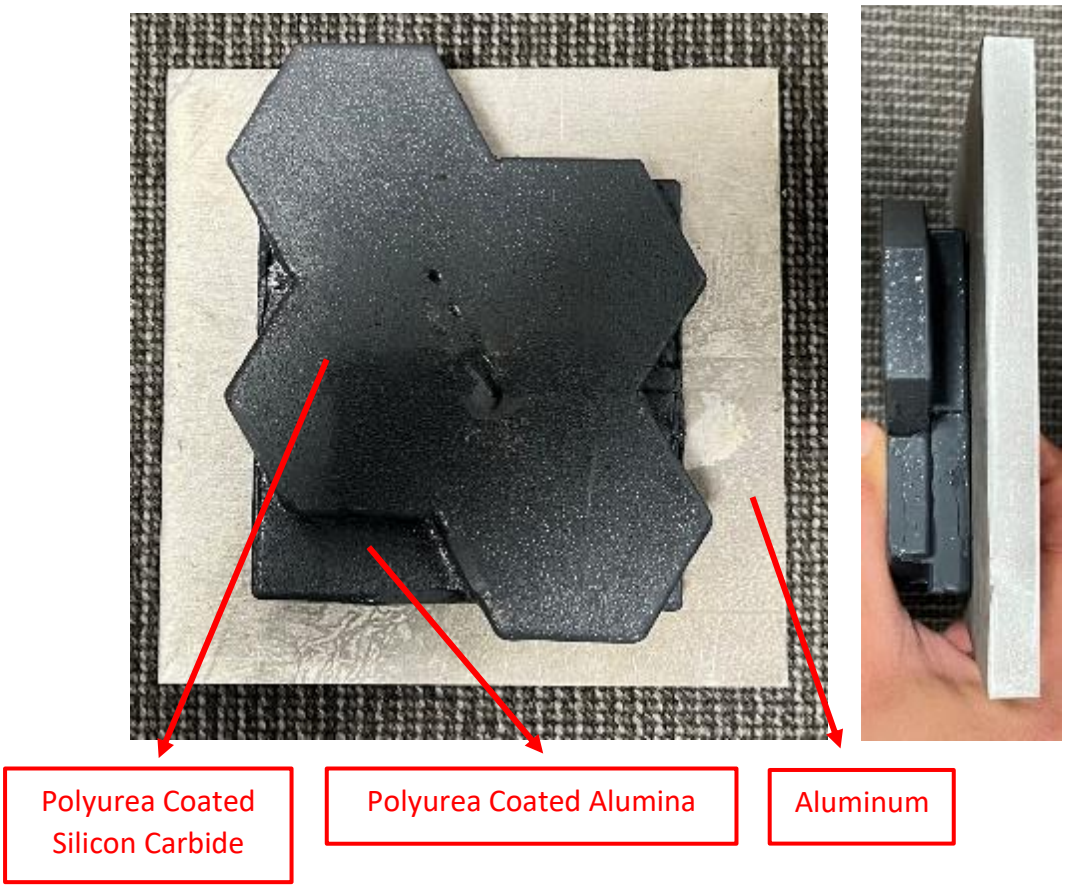

Figure 4.5. Physical Visual of Configuration – 4

In Configuration – 4, ballistic performance effect of the use of preliminary steel front layer has been tried to be examined by comparing Configuration – 4 and Configuration – 3. Silicon carbide layer used as a first ceramic layer and the ballistic performance effect of the sequencing of the alumina and silicon carbide layers has been investigated.

The detailed information of the Configuration – 5 is shown on Table 4.6, and the physical representation of the Configuration – 5 is shown on Figure 4.6:

Table 4.6. Schematic Diagram of Configuration – 5

Configuration – 5			
Front Layer	**Ceramic Core – 1**	**Ceramic Core – 2**	**Back Plate**
Steel Armor 150 x 150 mm 4 mm thickness	Alumina[3] 100 x 100 mm 10 mm thickness	Silicon Carbide[2] 100 x 100 mm 10 mm thickness	Aluminum Armor 150 x 150 mm 13 mm thickness

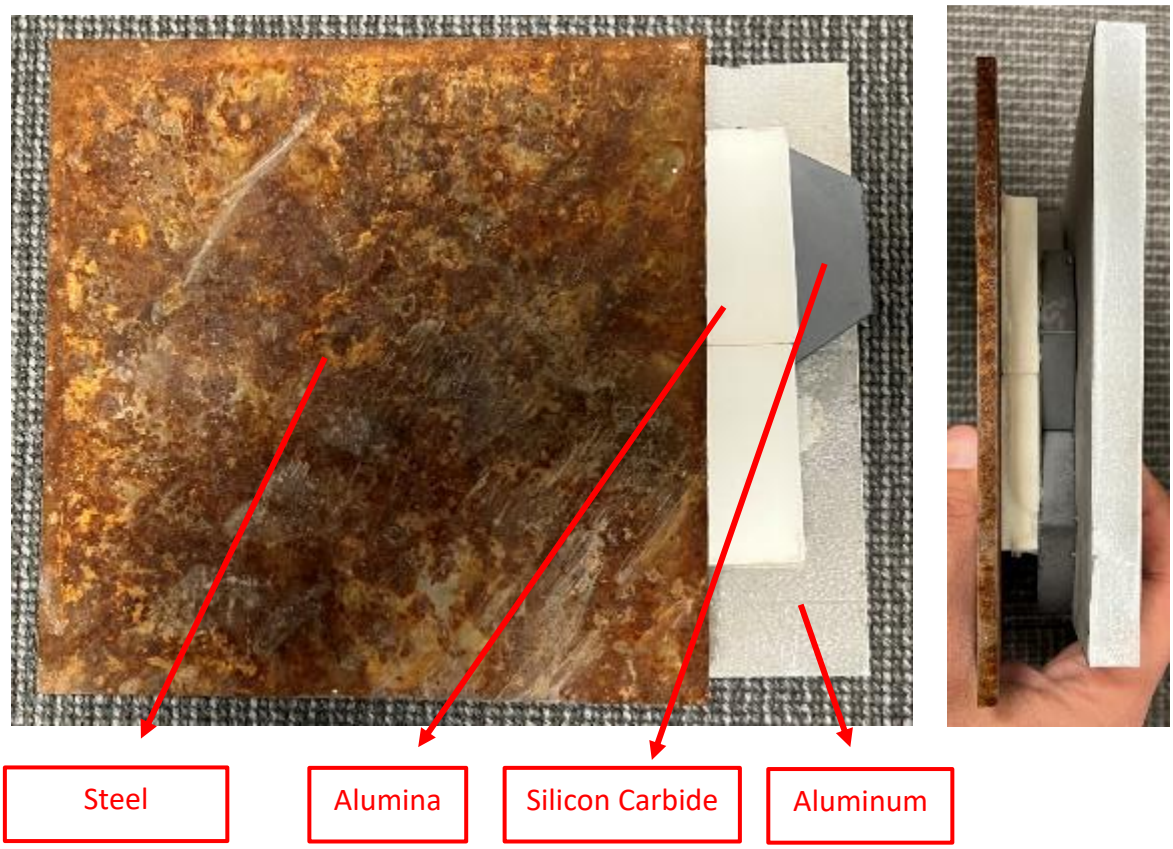

Figure 4.6. Physical Visual of Configuration – 5

In Configuration – 5, steel layer used as a preliminary layer and ballistic performance effect of the use of preliminary steel front layer has been tried to be examined. Alumina layer used as a first ceramic layer and the ballistic performance effect of the sequencing of the alumina and silicon carbide layers has been investigated by comparing Configuration – 5 and Configuration – 3.

The detailed information of the Configuration – 6 is shown on Table 4.7, and the physical representation of the Configuration – 6 is shown on Figure 4.7:

Table 4.7. Schematic Diagram of Configuration – 6

Configuration – 6			
Front Layer	**Ceramic Core – 1**	**Ceramic Core – 2**	**Back Plate**
Polyurea Coating ≈ 1 mm thickness	Alumina[3] 100 x 100 mm 10 mm thickness	Silicon Carbide[2] 100 x 100 mm 10 mm thickness	Aluminum Armor 150 x 150 mm 13 mm thickness

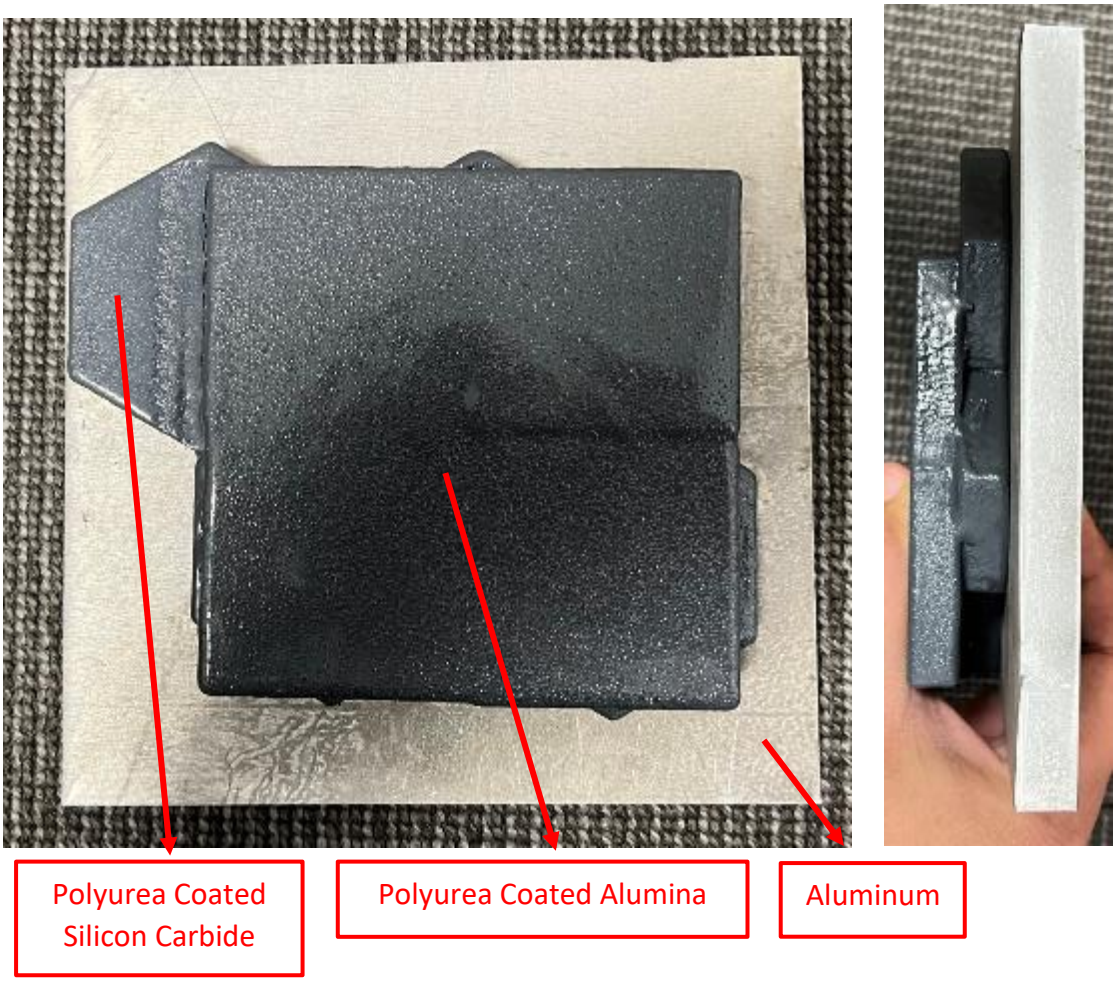

Figure 4.7. Physical Visual of Configuration – 6

[2]30 mm x 30 mm hexagon tiles (total 4 ea) were used in Configuration – 3, 4, 5 & 6.

[3]50 mm x 50 mm square tiles (total 4 ea) were used in Configuration – 3, 4, 5 & 6.

In Configuration – 6, ballistic performance effect of the use of preliminary steel front layer has been tried to be examined by comparing Configuration – 6 and Configuration – 5. Alumina layer used as a first ceramic layer and the ballistic performance effect of the sequencing of the alumina and silicon carbide layers has been investigated by comparing Configuration – 6 and Configuration – 4.

4.1. Preparation of Test Configurations

Firstly, steel and aluminum armor plates were prepared. Steel armor plate were cut with waterjet machine and aluminum armor plate were cut with Computer Numerical Control (CNC) saw machine. Cutting operations are shown in Figure 4.8 and Figure 4.9, respectively.

Figure 4.8. Steel Cutting Process with Waterjet

Figure 4.9. Aluminum Cutting Process with CNC Saw Machine

After cutting processes were completed both for steel and aluminum armor plates, sandpapering was applied to the steel armor samples for cleaning of rusty surface layer. Secondly, ceramic tiles were bonded with heat-activated adhesive. Bonded operation was shown in Figure 4.10.

Figure 4.10. Bonding of Ceramic Tiles

After bonding completion, 3 of 6 samples were coated with polyurea as shown in Figure 4.11

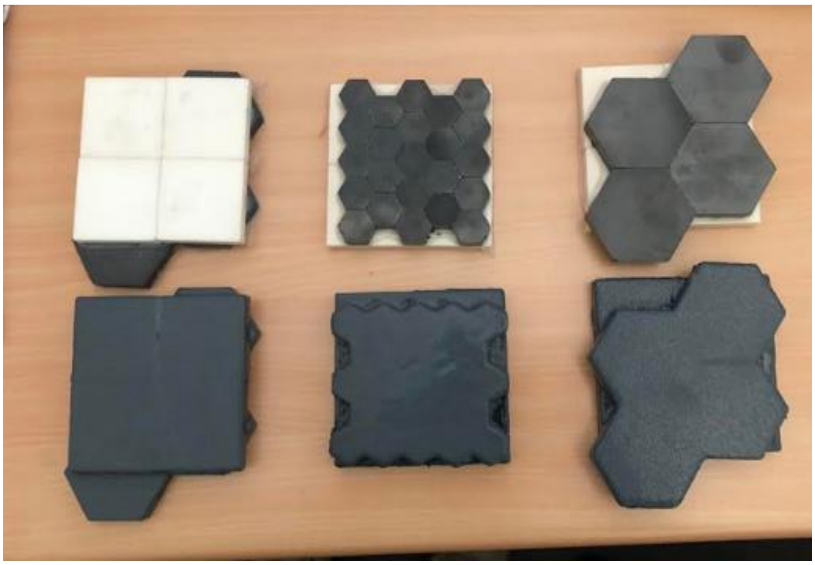

Figure 4.11. Coated and Uncoated Ceramic Tiles

Thirdly, in order to get ceramic samples in a square shape, epoxy resin was added into gaps by using 150 mm x 150 mm molding frame as shown in Figure 4.12.

Figure 4.12. Epoxy Resin Application to Ceramic Tiles

Lastly, after completion of every single ceramic tiles, all samples were ready for making sandwich framework. Steel, aluminum and ceramic samples were gathered and aluminum framework was obtained by using aluminum welding. Aluminum L profiles were used in back surfaces of configurations in order to get enough area both for impact and if applicable penetration. By doing so, fixed boundary conditions simulating real armor packages have been provided during the tests.

4.2. Calculations of Areal Densities of Configurations

4.2.1. Areal Density of Steel Front Layer:

Dimension and mass values for the calculation of areal density of steel front layer was given in Figure 4.13.

Figure 4.13. Dimensions and Mass of the Steel Front Layer

Width of the Steel Front Layer: 0,15 m

Height of the Steel Front Layer: 0,15 m

Mass of the Steel Front Layer: 0,811 kg

Areal Density of the Steel Front Layer: 36,04 kg/m^2

4.2.2. Areal Density of Silicon Carbide Layers:

Dimension and mass values for the calculation of areal density of 30 mm x 30 mm SiC hexagon tiles are given in Figure 4.14.

Figure 4.14. Dimensions and Mass of the 30 mm x 30 mm SiC Hexagon Tiles

Edge Length of the 30 mm x 30 mm SiC Hexagon Tiles: 0,03 m

Mass of the 30 mm x 30 mm SiC Hexagon Tiles: 0,063 kg

Areal Density of the 30 mm x 30 mm SiC Hexagon Tiles: 26,94 kg/m^2

Dimension and mass values for the calculation of areal density of 10 mm x 10 mm SiC hexagon tiles are given in Figure 4.15.

Figure 4.15. Dimensions and Mass of the 10 mm x 10 mm SiC Hexagon Tiles

Edge Length of the 10 mm x 10 mm SiC Hexagon Tiles: 0,01 m

Mass of the 30 mm x 30 mm SiC Hexagon Tiles: 0,011 kg

Areal Density of the 10 mm x 10 mm SiC Hexagon Tiles: 42,34 kg/m^2

4.2.3. Areal Density of Alumina Layer:

Dimension and mass values for the calculation of areal density of alumina tiles are given in Figure 4.16.

Figure 4.16. Dimensions and Mass of the Alumina Tiles

Width of the Alumina Layer: 0,05 m

Height of the Alumina Layer: 0,05 m

Mass of the Alumina Layer: 0,099 kg

Areal Density of the Alumina Layer: 39,60 kg/m^2

4.2.4. Areal Density of Aluminum Backing Layer:

Dimension and mass values for the calculation of areal density of aluminum backing layer are given in Figure 4.17.

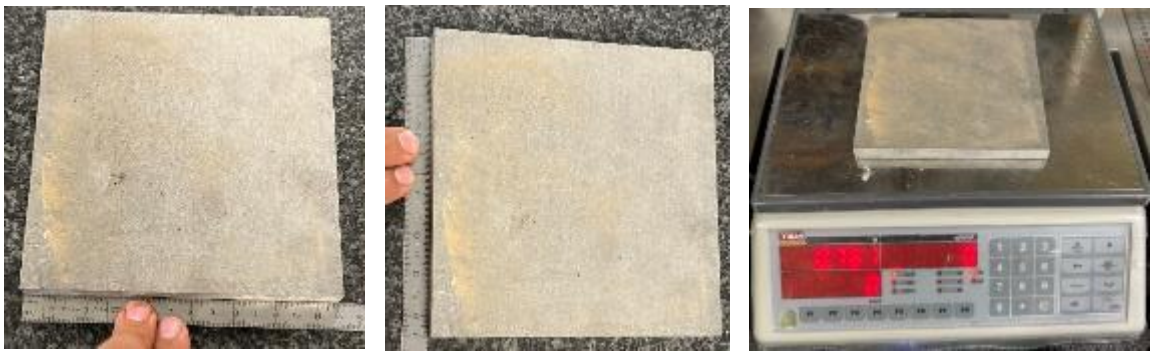

Figure 4.17. Dimensions and Mass of the Aluminum Backing Layer

Width of the Aluminum Backing Layer: 0,15 m

Height of the Aluminum Backing Layer: 0,15 m

Mass of the Aluminum Backing Layer: 0,781 kg

Areal Density of the Aluminum Backing Layer: 34,71 kg/m^2

Areal density values are summarized in Table 4.8 for each configuration.

Table 4.8. Areal Densities of Configurations

Configuration No	Areal Density (kg/m^2)
1	152,69
2	116,65
3	137,29
4	101,25
5	137,29
6	101,25

4.3. Test Preparations and Results

Trial shootings were performed for the determination of required gunpowder to reach the nominal velocity that given in STANAG 4569 for KE (Tungsten Carbide) Level-3 treat which is 930 ± 20 m/s. After stabilization shootings, Trial Configuration – 1 and Trial Configuration – 2 were assembled to the target panel by using additional clamps. Witness sample which is simulating the human body, also fixed behind the test samples. Assembly detail of Trial Configuration – 2 is given in Figure 4.18.

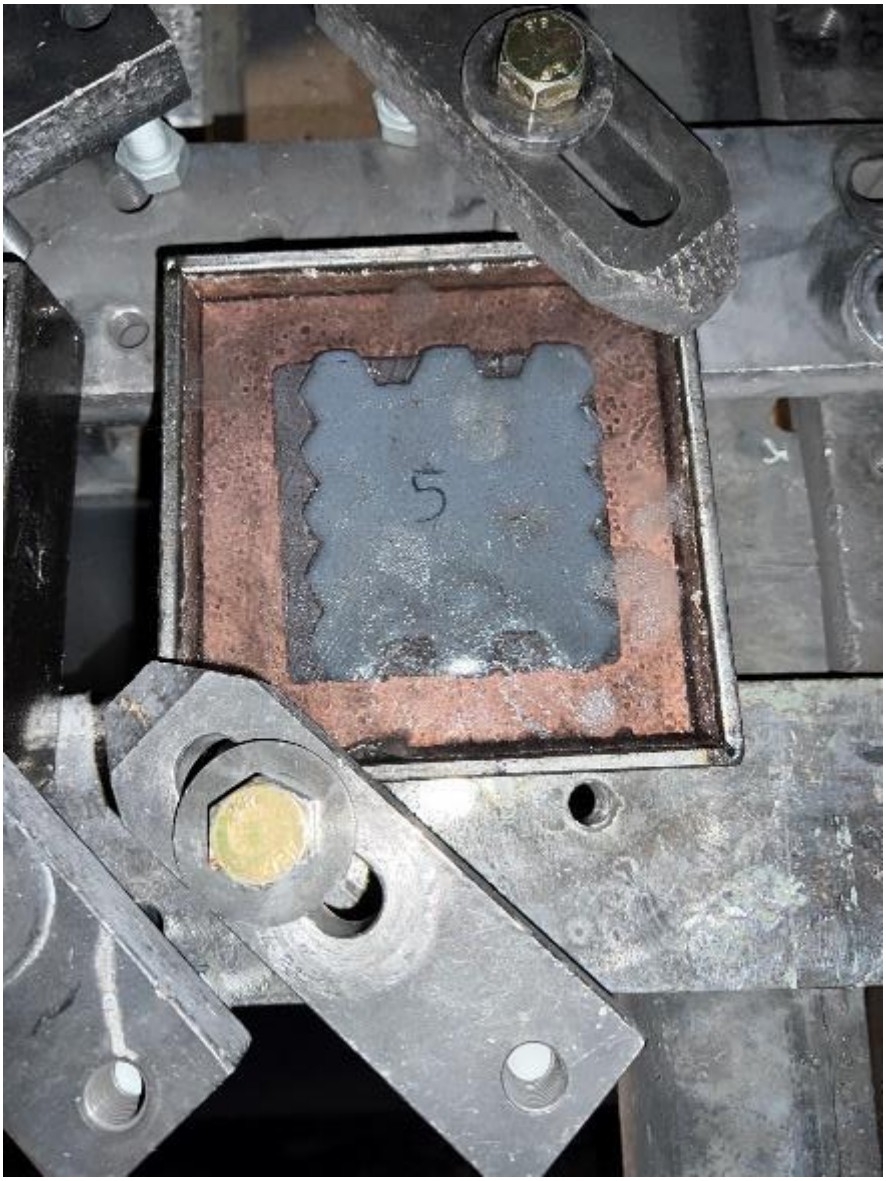

Figure 4.18. Assembly of Trial Configuration – 2 to the Test Panel

After completion of assembly activities, 2 shootings were performed to each trial configuration (1 & 2) for observation of complete penetration or partial penetration situations. It is obtained that both Trial Configuration – 1 and Trial Configuration – 2 stopped the projectile. Once this information was obtained, remaining tests were performed with the same test conditions (STANAG 4569 KE (Tungsten Carbide) Level-3 treat). Because, as mentioned before, Trial Configuration – 1 & 2 were created for detection of proper impact velocity and ballistic protection level. Detailed test visual of front plate of Trial Configuration – 1 after 2 shooting is given in Figure 4.19.

Figure 4.19. Front Plate Visual of Configuration – 1 after Shootings (Impact Velocities: 942 m/s and 940 m/s)

According to the examinations, impact marks were observed on backing plate of Trial Configuration – 1. Detailed visuals of front layer, ceramic core – 1 and back plate of Trial Configuration – 1 is given in Figure 4.20.

Figure 4.20. Detailed Visuals of Trial Configuration – 1 after Ballistic Impact (Front Layer, Ceramic Core – 1 & Back Plate)

Depth of penetration calculations for Trial Configuration – 1 are shown in Figure 4.21 and Figure 4.22

Figure 4.21. Depth of Penetration on Backing Plate After First Impact of Trial Configuration – 1 (0,34 mm)

Figure 4.22. Depth of Penetration on Backing Plate After Second Impact of Trial Configuration – 1 (0,24 mm)

Detailed test visuals of ceramic core – 1 and back plate of Trial Configuration – 2 after 2 shooting was given in Figure 4.23. According to the examinations, impact marks were observed on backing plate of Trial Configuration – 2 as also can be shown in Figure 4.23.

Figure 4.23. Detailed Visuals of Trial Configuration – 2 after Ballistic Impact (Impact Velocities: 936 m/s and 929 m/s)

Depth of penetration calculations for Trial Configuration – 2 are shown in Figure 4.24 and Figure 4.25.

Figure 4.24. Depth of Penetration on Backing Plate After First Impact of Trial Configuration – 2 (1,93 mm)

Figure 4.25. Depth of Penetration on Backing Plate After Second Impact of Trial Configuration – 2 (2,77 mm)

It was observed that, silicon carbide and alumina tiles of Trial Configuration – 1 stayed together after 2 impacts. But, tiles were broken into pieces around the impact zone in Trial Configuration – 2 as shown in Figure 4.26.

Figure 4.26. Broken Ceramic Tiles of Trial Configuration – 2 after Ballistic Impact

After completion of trial tests on Trial Configuration – 1 & 2, remaining samples were assembled the target panel and ballistic tests were performed by using all remaining configurations.

Detailed test visual of front plate of Configuration – 3 after 2 shooting is given in Figure 4.27.

Figure 4.27. Front Plate Visual of Configuration – 3 after Shootings (Impact Velocities: 914 m/s and 922 m/s)

According to the examinations, impact mark related to second impacts was observed on backing plate of Configuration – 3. Detailed visual of front layer, ceramic core – 1 and back plate of Configuration – 3 is given in Figure 4.28

Figure 4.28. Detailed Visual of Configuration – 3 after Ballistic Impact (Front Layer, Ceramic Core – 1 & Back Plate)

Depth of penetration calculations for Configuration – 3 are shown in Figure 4.29 and Figure 4.30.

Figure 4.29. Depth of Penetration on Configuration – 3 After First Impact (13,46 mm from surface)

Figure 4.30. Depth of Penetration on Backing Plate After Second Impact of Configuration – 3 (0,23 mm)

According to the test results of the first impact, projectile was stopped by first ceramic layer (silicon carbide) since total thickness value of preliminary steel armor and first ceramic layer equals to 14 mm for Configuration – 3 as shown in Figure 4.29. But for the second impact, projectile was stopped by backing plate.

Detailed test visuals of ceramic core – 1 and back plate of Configuration – 4 after 2 shootings was given in Figure 4.31. According to the examinations, no impact marks were observed on backing plate of Configuration – 4 as also can be shown in Figure 4.31.

Figure 4.31. Detailed Visuals of Configuration – 4 after Ballistic Impact (Impact Velocities: 930 m/s and 904 m/s)

Depth of penetration could not be measured since silicon carbide and alumina tiles in Configuration – 4 completely break into pieces after ballistic impact as shown in Figure 4.32.

Figure 4.32. Broken Ceramic Tiles of Configuration – 4 after Ballistic Impact

Detailed test visuals of front plate and back plate of Configuration – 5 was given in Figure 4.33. According to the examinations, impact marks were observed on backing plate in Configuration – 5 as shown in Figure 4.33.

Figure 4.33. Detailed Visuals of Configuration – 5 after Ballistic Impact (Impact Velocities: 933 m/s and 934 m/s)

Depth of penetration calculations for Configuration – 5 are shown in Figure 4.34 and Figure 4.35.

Figure 4.34. Depth of Penetration on Backing Plate After First Impact of Configuration – 5 (0,29 mm)

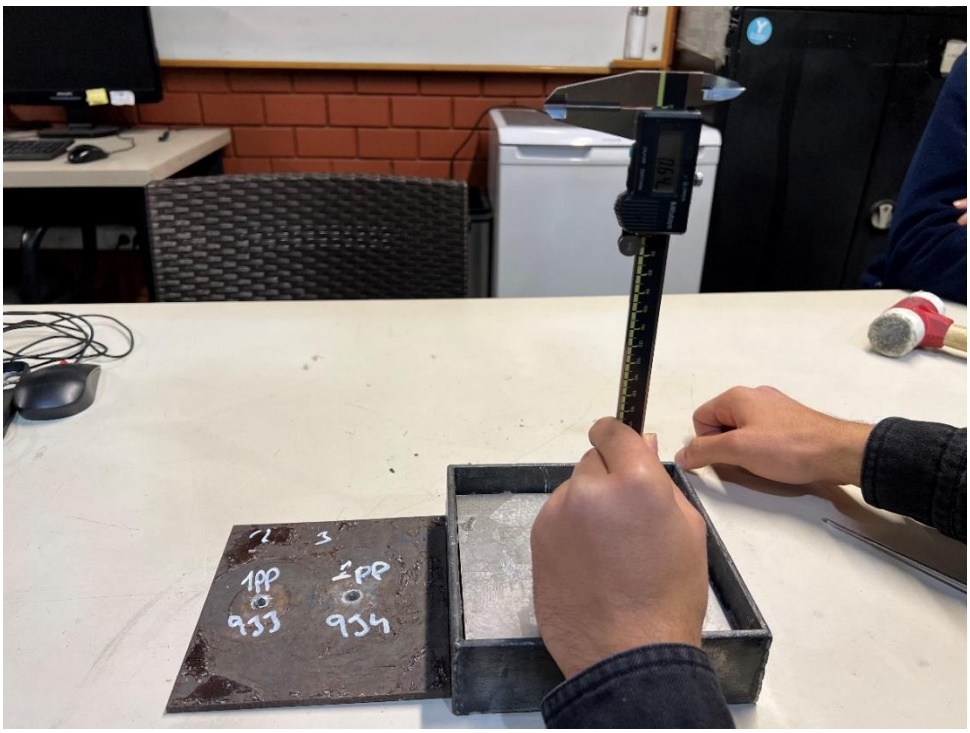

Figure 4.35. Depth of Penetration on Backing Plate After Second Impact of Configuration – 5 (0,64 mm)

According to the test results of the both first and second impacts, projectile was stopped by backing plate.

Detailed test visuals of ceramic core – 1 and back plate of Configuration – 6 after 2 shootings was given in Figure 4.36. Impact marks which were observed on backing plate in Configuration – 6 are given in Figure 4.36

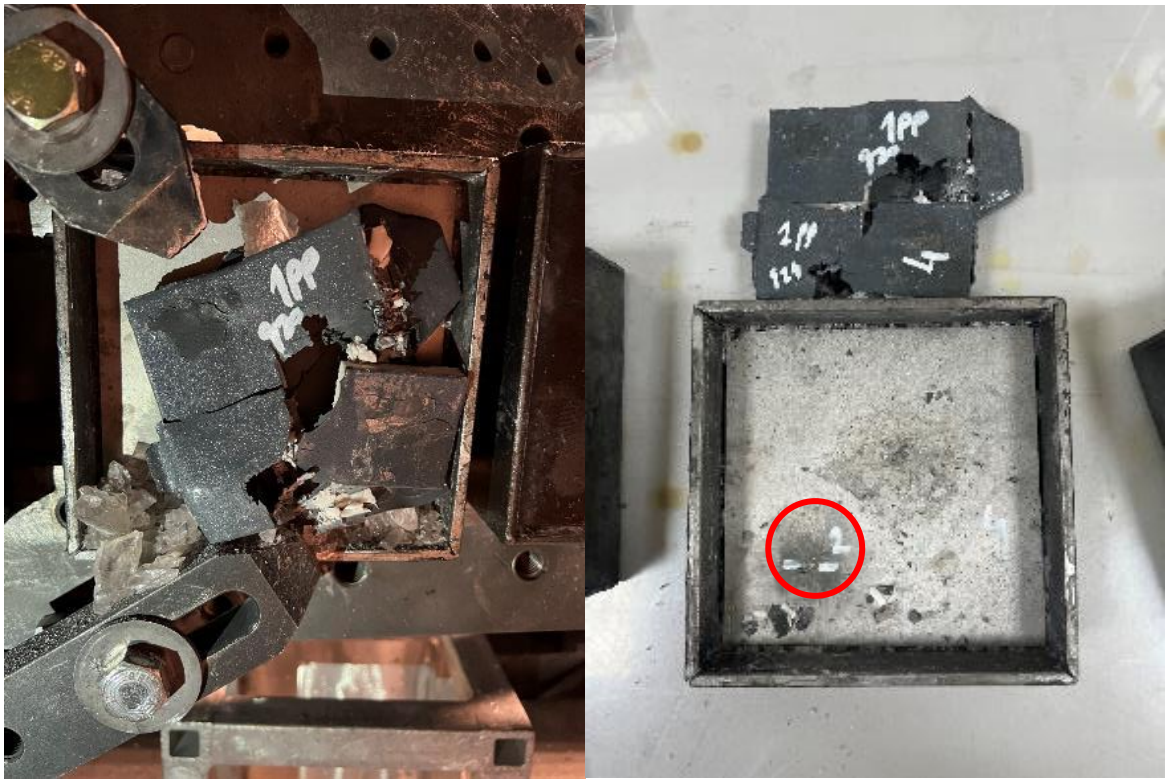

Figure 4.36. Detailed Visuals of Configuration – 6 (Impact Velocities: 920 m/s and 924 m/s)

According to the examinations, impact mark was observed on backing plate caused by second impact in Configuration – 6. But, depth of penetration could not be measured for the first impact since ceramic tiles of both layers completely separated as shown in Figure 4.36 and Figure 4.38.

Depth of penetration calculation for the second impact of the Configuration – 6 is shown in Figure 4.37.

Figure 4.37. Depth of Penetration on Backing Plate After Second Impact of Configuration – 6 (1,58 mm)

It was observed that, alumina and silicon carbide tiles in Configuration – 6 completely break into pieces after ballistic impact as shown in Figure 4.38

Figure 4.38. Broken Ceramic Tiles of Configuration – 6 after Ballistic Impact

4.4. Evaluations of Experimental Studies

- Using preliminary front steel armor layer have positive effect on ballistic performance (by comparing Trial Configuration – 1 versus Trial Configuration – 2 and Configuration – 5 versus Configuration – 6 for the second impact)
- Using preliminary front layer have positive effect on multi-hit capability of armor systems since front layer keeps ceramic layers together. Otherwise, ceramic tiles of Configuration – 2 (Trial), 4 & 6 fully break into pieces after ballistic impacts.
- Using silicon carbide ceramic layer as a first ceramic layer instead of alumina have positive effect on ballistic performance (by comparing Configuration – 3 versus Configuration – 5 and Configuration – 4 versus Configuration – 6). It is evaluated that, if the projectile interacts with a higher strength ceramic layer firstly, erosion amount of the projectile increases accordingly.
- According to the test results which were given in Table 4.9, it was observed that Configuration – 4 showed the best ballistic performance with minimum areal density. But since ceramic tiles fully break into pieces in Configuration – 4, it is seen that the multi hit capability of this configuration is low.
- According to the test results which were given in Table 4.9, when considering the multi-hit capability, it was observed that Configuration – 3 showed best ballistic performance since only one mark related to second impact was observed on back plate. However, it has been observed that the areal density of this configuration is high.
- According to the test results which were given in Table 4.9, Configuration – 5 showed the lowest ballistic performance with higher areal density, which is not desired for the weight reduction consideration.
- Number of samples should be increased for obtain more precise results. According to the test results, there were cases where lower depth of penetration was obtained at higher impact velocities especially for the second impacts. It is evaluated that, pressure and fractures that occurred after the first impact effect the nearby ceramic tiles. It causes decrease on ballistic performance in second impact.
- Taking all the results into consideration which were given in Table 4.9, since one of the most significant constraint of the armor design is the areal density and mass, it is evaluated that the Configuration – 4 is the best configuration for the armored personnel carriers within in the scope of this study.

Experimental results summarized in Table 4.9 for each configuration.

Table 4.9. Summary of Experimental Results

Configuration No	**First Impact Velocity (m/s)**	**Second Impact Velocity (m/s)**	**Total Depth of Penetration for First Impact (mm)**	**Total Depth of Penetration for Second Impact (mm)**	**Observation on Backing Plate**	**Observation of Ceramic Tiles**	**Areal Density (kg/m^2)**
Trial Configuration – 1	942	940	24,34	24,24	Marks were observed for both impacts	Broken but stayed together	152,69
Trial Configuration – 2	936	929	22,93	23,77	Marks were observed for both impacts	Completely broken into pieces	116,65
Configuration – 3	914	922	17,46	24,23	Mark was observed only for second impact	Broken but stayed together	137,29
Configuration – 4	930	904	Estimated: Between 11-21	Estimated: Between 11-21	No marks were observed for both impacts	Completely broken into pieces	101,25
Configuration – 5	933	934	24,29	24,64	Marks were observed for both impacts	Broken but stayed together	137,29
Configuration – 3	920	924	Estimated: Between 11-21	22,58	Mark was observed only for second impact	Completely broken into pieces	101,25

5. ANALYTICAL CALCULATIONS

5.1. Required Parameters for Analytic Solutions

Parameters which were used in calculations were taken from different references and they are given in Table 5.1:

Table 5.1. Other Parameters That are Used in Calculations

Property	Value	Unit	Reference
Projectile Mass/Initial Mass	0,072	kg	[14]
Diameter of Projectile	0,012	m	[14]
Yield Strength of the Armor Steel	1100	MPa	SSAB official web site
Density of the Armor Steel	9011,11	kg/m^3	Calculated according to the values that given "Areal Density of Steel Front Layer" section
Impact Velocity	930	m/s	STANAG 4569
Nose Length of the Projectile	0,01526	m	Figure 5.1
Density of the Projectile	18.100	kg/m^3	[14]
Dynamic Yield Strength of Projectile	2,4	GPa	[14]
Hugoniot Elastic Limit (HEL) of the Silicon Carbide	15	GPa	[15]
Hugoniot Elastic Limit (HEL) of the Alumina	7	GPa	[15]
Shear Strength of Silicon Carbide	350	MPa	[15]
Shear Strength of Alumina	300	MPa	[15]

Figure 5.1. Measurement of Nose Length of the Projectile

5.2. Calculations

Calculations were completed by using the parameters that were given in section 5.1. Results are given in Table 5.2, Table 5.3, Table 5.4 and Table 5.5 for the Configuration – 3, 4, 5 and 6 respectively.

Table 5.2. Analytical Calculations for Configuration – 3

Description	Configuration No	Analytical Method	Results
Ballistic Limit of Preliminary Steel Armor Layer	3	Pol Model	119,12 m/s
Residual Velocity of Projectile (after Preliminary Steel Armor Layer)		Lambert-Jonas Model	874,70 m/s
Residual Velocity of Projectile (after first Silicon Carbide Layer)		Tang & Wen Model	614,76 m/s
Residual Velocity of Projectile (after second Alumina Layer)		Tang & Wen Model	-(1)

(1) According to the Tang & Wen Model, if minus value obtained as a result of analytical calculations, it means projectile was halted by the ceramic layer that was used in analytical calculations.

Table 5.3. Analytical Calculations for Configuration – 4

Description	Configuration No	Analytical Method	Results
Residual Velocity of Projectile (after first Silicon Carbide Layer)	4	Tang & Wen Model	665,99 m/s
Residual Velocity of Projectile (after second Alumina Layer)		Tang & Wen Model	-[(1)]

[(1)] According to the Tang & Wen Model, if minus value obtained as a result of analytical calculations, it means projectile was halted by the ceramic layer that was used in analytical calculations.

Table 5.4. Analytical Calculations for Configuration – 5

Description	Configuration No	Analytical Method	Results
Ballistic Limit of Preliminary Steel Armor Layer	5	Pol Model	119,12 m/s
Residual Velocity of Projectile (after Preliminary Steel Armor Layer)		Lambert-Jonas Model	874,70 m/s
Residual Velocity of Projectile (after first Alumina Layer)		Tang & Wen Model	644,98 m/s
Residual Velocity of Projectile (after second Silicon Carbide Layer)		Tang & Wen Model	-[(1)]

[(1)] According to the Tang & Wen Model, if minus value obtained as a result of analytical calculations, it means projectile was halted by the ceramic layer that was used in analytical calculations.

Table 5.5. Analytical Calculations for Configuration – 6

Description	Configuration No	Analytical Method	Results
Residual Velocity of Projectile (after first Alumina Layer)	6	Tang & Wen Model	689,27 m/s
Residual Velocity of Projectile (after second Silicon Carbide Layer)		Tang & Wen Model	-[(1)]

[(1)] According to the Tang & Wen Model, if minus value obtained as a result of analytical calculations, it means projectile was halted by the ceramic layer that was used in analytical calculations.

6. RESULTS AND DICUSSION

6.1. Comparison of Experimental and Analytical Results

- According to the experimental results given in Table 4.9 as well as the analytical results given in Table 5.2 through Table 5.5, all configurations stopped the projectile that means no perforation.
- According to the analytical results that were given in Table 5.2 through Table 5.5, it has been observed that the configurations in which silicon carbide is used as the first layer has higher ballistic performance when compared to the configurations where alumina is used as the first layer, very similar results with experimental results that were given in Table 4.9 when areal density was not considered in the assessment.
- When areal density was not considered in the assessment, according to the analytical results that were given in Table 5.2 through Table 5.5, configurations containing preliminary steel armor layer showed better ballistic performance when comparing them with configurations without preliminary steel armor layer. But according to the experimental results that were given in Table 4.8, Configuration – 4 which is not containing preliminary steel armor layer, showed the best ballistic performance.
- According to the results of the experimental studies, impact marks were found on the backing plate in almost all configurations. However, according to analytical results, all configurations stop the projectile in the second ceramic layer.
- As can be seen in the results of analytical calculations, projectiles were halted by the second ceramic layer for all configurations. For this reason, an accurate depth of penetration determination is not possible. Within this scope, comparison of analytical and experimental results will be more amenable considering the situations of partial penetrated or perforated instead of depth of penetration values.

6.2. Evaluation of Results

- Since residual velocity could not be measured during ballistic tests because of the lack of infrastructure, results of Pol and Lambert-Jonas models could not be verified one by one. But, according to the conclusive calculations of all models, no complete penetration (CP) was observed in any configuration. Also, similar results obtained during the ballistic tests. Based on these results, it can be evaluated that the models

used in the study were considered to be suitable for the ceramic/composite armor configurations which are containing two ceramic layers.

- According to the experimental results given in Table 4.9, Configuration – 4 which does not contain preliminary steel armor layer, showed the best ballistic performance on the basis of areal density like analytical calculations. Based on analytical results, it was evaluated that the amount of erosion that observed on the projectile has significant effect on ballistic performance. In other words, with respect to material characteristics, the effect of silicon carbide layer on erosion amount of projectile is higher when compared with both steel and alumina layers. That is why residual velocity after silicon carbide is higher (665,99 m/s) for the configuration without front steel layer (Config-4) than the residual velocity of after silicon carbide (614,76 m/s) for the configuration with front steel layer (Config-3)
- Since use of silicon carbide layer as the first layer increases the amount of erosion in the bullet, it has been determined that the ballistic performance of these configurations is higher than the configurations that use alumina as the first layer.
- Relatively small test samples were prepared due to limited supply capability. Therefore, it has been observed that the pressure effect after the first impact related to breakage of ceramic tiles seriously affects the ballistic performance of the overall configuration. This is thought to be the reason why second impacts with lower velocities create a deeper depth of penetration.

7. CONCLUSION

- All samples configurations were successfully to halt the projectile according STANAG 4569 Level 3 ballistic test specifications.
- According to the test results, it was obtained that the configuration with the highest ballistic performance was the Configuration – 4 with respect to lowest areal density.
- In comparison with general literature studies, it has been revealed that the use of two ceramic layers on top of each other can be an engineering solution to achieve high ballistic performance.
- The first impact of the projectile on a layer having higher hardness increases the amount of erosion of the projectile and accordingly the ballistic performance. Considering the materials used in the study, the material with the highest hardness property is silicon carbide. As can be seen in Table 4.9, Configuration – 4 which containing silicon carbide as a first layer showed to best ballistic performance. As a result of this, the importance of using materials with high hardness properties as the first layer in armor solutions has been demonstrated.
- With respect to areal density values, it was determined that Configuration – 4 and Configuration – 6 would be the best armor design solutions since no complete penetration was observed in any configuration according to the experimental results. When these two configurations are compared, it has been determined that the Configuration – 4 has higher ballistic performance as mentioned before. Because, no marks were observed after two impact on backing plate of Configuration – 4.
- It has been observed that the use of a preliminary steel front layer increases the multi-hit capability of the configurations. However, according to the test results that given in Table 4.9, it was seen that this situation did not have a positive effect on ballistic performance if areal density is considered. On the contrary, it was observed that the areal density is increased and the ballistic performance is decreased slightly in the configurations which are containing preliminary steel front layer.
- As mentioned in section 6.1, it can be seen that comparison of analytical and experimental results will be more amenable considering the situations of partial penetrated or perforated instead of depth of penetration values.
- Since ceramic armors are more expensive than steel and aluminum armors, a relatively expensive solution has been obtained within the scope of this study. In

order to obtain a cheaper solution, it is thought that configuration optimization such as:

- Decreasing thickness of ceramic tiles since there is no complete penetration observed during experimental studies,
- Increasing the thickness of the backing plate and canceling the front steel plate but coating the ceramics with Polyurea to protect the ceramic from outside effects.

should be considered and tested.

REFERENCES

[1] R. Zaera & V. Sanchez-Galvez. Analytical Modelling of Normal and Oblique Ballistic Impact on Ceramic/Metal Lightweight Armors. *Int. J. Impact Engng Vol. 21, No. 3*, 133-148, 1997.

[2] Fabio de Oliveira Braga, Fernanda Santos da Luz, Sergio Neves Monteiro & Edio Pereira Lima Jr. Effect of the Impact Geometry in the Ballistic Trauma Obsorption of a Ceramic Multilayered Armor System. *Journals of Materials Research and Technology*, 54-60, 2018.

[3] Yanfei Yang & Xiaogang Chen. Investigation on Energy Absorption Efficiency of Each Layer in Ballistic Amour Panel for Applications in Hybrid Design. *Composite Structures 164*, 1-9, 2017.

[4] Fabio de Oliveira Braga, Edio Pereira Lima Jr., Eduardo de Sousa Lima & Sergio Neves Monteiro. The Effect of Thickness on Aramid Fabric Laminates Subjected to 7.62 MM Projectile Ballistic Impact. *Materials Research 20 Suppl. 2*, 676-680, 2017.

[5] Prince Sharma, Pradeep Chandel, Puneet Mahajan & Manjit Singh. Quasi-Brittle Fracture of Aluminium Alloy 2014 under Ballistic Impact. *Procedia Engineering 173*, 206-213, 2016.

[6] Fabio de Oliveira Braga, Pedro Henrique L. M. Lopes, Michelle Souza Oliveira, Sergio Neves Monteiro & Edio Pereira Lima Jr. Thickness Assessment and Statistical Optimization of a 3-Layerd Armor System with Ceramic Front and Curaua Fabric Composite/Aluminum Alloy Backing. *Composites Part B 166*, 48-55, 2019.

[7] Li Jinzhu, Zhang Liansheng & Huang Fenglei. Experiments and Simulations of Tungsten Alloy Rods Penetrating into Alumina Ceramic/603 Armor Steel Composite Targets. *International Journal of Impact Engineering 101*, 1-8, 2017.

[8] Artur Camposo Pereira, Foluke Salgado de Assis, Fabio da Costa Garcia Filho, Michelle Souza Oliveira, Luana Cristyne da Cruz Demosthenes, Henry Alonso Colorado Lopera & Sergio Neves Monteiro. Ballistic Perofrmance of Multilayered Armor with Intermediate Polyester Composite Reinforced with Fique Natural Fabric and Fibers. *Journals of Materials Research and Technology*, 4221-4226, 2019.

[9] W. L. Goh, Y. Zheng, J. Yuan & K. W. Ng. Effects of Hardness on Ceramic Amour Module Against Long Rod Impact. *International Journal of Impact Engineering 109*, 419-426, 2017.

[10] N. Nsiampa, G. Dyckmans & A. Chabotier. Impact of 7.62 MM AP Projectile into Aluminium 5083 Plates. *23RD International Symposium on Ballistics Tarragona*, 2007.

[11] A. Tasdemirci, G. Tunusoglu & M. Güden. The Effect of the Interlayer on the Ballistic Performance of Ceramic/Composite Armors: Experimental and Numerical Study. *International Journal of Impact Engineering 44*, 1-9, 2012.

[12] M. H. Pol, A. Bidi, A. V. Hoseini & G. H. Liaghat. Analysis of Normal Penetration of Ogive - Nose Projectiles into Thin Metallic Plates: *World Academy of Science, Engineering and Technology International Journal of Mechanical and Mechatronics Engineering, Vol:3, No:2,* 145-148, 2009.

[13] J. P. Lambert G. H. Jonas. Towards Standardization Of In Terminal Ballistic Testing: Velocity Representation: *World Academy of Science, Ballistic Research Laboratory, Report No: 1852,* 1976.

[14] R. T. Tang & H. M. Wen. Predicting the Perforation of Ceramic-Faced Light Armors Subjected to Projectile Impact: *International Journal of Impact Engineering 102*, 55-61, 2017.

[15] T. J. Holmquist, A. M. Rajendran, D. W. Templeton & K. D. Bishnoi. A Ceramic Armor Material Database: *TARDEC Technical Report*. No: 13754, 1999.